A STUDY OF IN-CYLINDER COMBUSTION PROCESSES BY USING HIGH SPEED MULTI-SPECTRAL INFRARED IMAGING AND A ROBUST STATISTICAL ANALYSIS METHOD

BY JOSEPH R VANDERVEER

A thesis submitted to the

Graduate School—New Brunswick

Rutgers, The State University of New Jersey

in partial fulfillment of the requirements

for the degree of

Master of Science

Graduate Program in Mechanical and Aerospace Engineering

Written under the direction of

Dr. KT Rhee

and approved by

_____

_____

_____

New Brunswick, New Jersey

January, 2008

ABSTRACT OF THE THESIS

A Study of In-Cylinder Combustion Processes by using High Speed Multi-Spectral Infrared Imaging and a Robust Statistical Analysis Method

by Joseph R VanderVeer
Thesis Director: Dr. KT Rhee

Combustion processes in a spark-ignition engine were studied by using a high speed multi-spectral infrared camera system and a new robust statistical analysis method. Among the variables in the experiment are fuel and fuel additives.

The images were obtained using Rutgers Super Imaging System, which consists of four spatial infrared cameras. The cameras are designed to be spatially aligned and their wavelengths are $3.8\mu m$, $2.09\mu m$, $3.48\mu m$, $2.47\mu m$. Each camera consists of a Pt-Si charge-coupled device with a pixel array of 64×64 and a depth of 12 bits.

The engine used is a 1999 Ford Mustang 4.6L engine. This engine was modified to allow optical access by means of a Bowditch method. The piston was redesigned for this study. Instead of graphite rings, metallic rings and oil lubricant were used to seal the combustion chamber.

A statistical analysis tool (CASAT) was developed to analyze infrared images. This tool included multiple methods for statistically analyzing the fuels, most notably the novel method time derivative spatial averaging (TDSA).

The ultimate goal of the research was to verify the capabilities of the TDSA method. This was achieved via a blind study, consisting of 10 unknown fuels; 2 base fuels and 8

fuels with additives. The results of the TDSA method predicted four fuels had various amounts of an octane improver, and the other four had a cetane improver. The actual results were octane improver and combustion enhancer. The effects of a cetane improver of gasoline and the effects of a combustion enhancer of gasoline are very similar.

Acknowledgements

I would like to thank everyone that has helped me on this long journey. I need to thank Dr. Rhee for his patience with my work and the long encouraging discussions we have had. The friends that have helped me, thank you. Kevin Gomes for your moral support and an ear to talk to when I had had it with my research. William Doig for your unending motivation to do something worthwhile when doing nothing seemed much more fun. Mārcis Jansons for sharing his wisdom as a graduate student. My parents for helping me financially when you could, and even sometimes when you couldn't. Thank you for believing that I could make it this far. Finally, to my wife, whom has put up with my never ending desire to finish my work. The long nights spent alone, and the long hours watching me type. Thank you for being there when I needed you the most.

Dedication

To my parents, for pushing me this far.

Table of Contents

List of Tables

List of Figures

List of Abbreviations

aBDC	after Bottom Dead Center
aTDC	after Top Dead Center
bBDC	before Bottom Dead Center
BDC	Bottom Dead Center
bTDC	before Top Dead Center
CASAT	Computer Assisted Statistical Analysis Tool
CCD	Charged Coupled Device
CPLD	Complex Programmable Logic Device
DOHC	Double Over-Head Cam
ID	Inside Diameter
IMEP	Indicated Mean Effective Pressure
LCD	Liquid Crystal Display
LUT	Look Up Table
OD	Outside Diameter
OEP	Original Extended Piston
OEM	Original Equipment Manufacturer
RAP	Rutgers Animation Program
REP	Redesigned Extended Piston
RIA	Rutgers Imaging Application
RPM	Revolutions Per Minute
SIS	Super Imaging System
TDC	Top Dead Center

Chapter 1

Introduction

> *I'd put my money on the sun and solar energy. What a source of power!*
> *I hope we don't have to wait 'til oil and coal run out before we tackle that.*
> *—Thomas Edison*

Unfortunately, the earth's oil resources are being used at an alarming rate. Alternative energy source technologies are progressing, although no hard scientific information yields a date to when this technology will be ready to supplant petroleum-based fuels as the dominant energy source [1]. Thus, work must be done to stretch the oil reserves as much as possible.

On November 17, 2005 an amendment was introduced to the Clean Air Act. This amendment would require all gasoline sold as a transportation fuel to be a minimum of 10% renewable fuels by 2010 (a.k.a. 10 by 10 act) [1]. This is obviously a step in the right direction, however, it may be an expensive one for the average driver.

Alternative fuels and fuel additives may enable the oil reserves to be stretched further. Open any book on internal combustion engines[1] and one will find many alternative fuels such as methanol also known as methyl alcohol or fuel additives such tetraethyl lead (TEL). However, what makes a fuel better than another fuel for an internal combustion engine? Is it a fuel that is the most efficient? Or a fuel that produces the most amount of power within an engine? The answers to these questions are difficult and very political in nature, however, a fuel does have certain characteristics which can be quantified, and subsequently classify the fuel and its additives.

---

[1]The term internal combustion engine or just engine has many different meanings. Throughout this text it shall be the of the reciprocating spark ignition internal combustion engine, commonly found in automobiles.

1.1   Motivation of This Work

Previous work on fuel additives have shown that a relatively insignificant quantity of a substance mixed with a fuel may drastically affect the combustion processes. This work has shown fuel properties such as octane rating, cetane rating, and emissions can be altered. Other, seemingly engine/environment specific properties may be altered using fuel additives, such as intake temperature, specific fuel consumption, engine power, and volumetric efficiency.

Cyclic variations of the internal combustion engine have been difficult to minimize. Seemingly perfect and identical situations yield completely different results. Cyclic variations are complicated phenomena which exact causes are still unknown, although they include: variations in mixture motion, variations in the fuel-air ratio, and variations in residual gases. Over the past few decades, much research has gone into understanding and reducing these variations.

Using a four-bandwidth 2D infrared imaging device, developed at the Internal Combustion Engines Research Laboratory at Rutgers University, one may record video of combustion as it occurs inside an engine (the experimental apparatus is described further in chapter 2). The camera system is capable of recording images from successive cycles for cyclic analysis.

A problem using this system is analyzing the data that is recorded. The imaging system, known as Rutgers Super Imaging System or SIS, produces an enormous amount of data at a rate of 31 MB per second (1-megabyte equals 1048576 bytes). A person would find this amount of data difficult to accurately analyze the data. For this reason, a computer application is required to analyze the data from SIS.

A library known as CASAT, short for Computer Assisted Statistical Analysis Tool, analyzes the data and organizes the information into easier to understand Excel files (CASAT is described in detail in chapter 6).

1.2 Previous Work

The following sections are on work previously done and documented in literature. It is broken into three sections: Fuels and Fuel Additives, Fuel Properties and Spectroscopic Analysis.

1.2.1 Fuels and Fuel Additives

Fuels and fuel additives, are difficult to logically group; a fuel can be a fuel additive and vice versa. The biggest difference is quantity; a fuel is typically used in large quantities, i.e. gallons, while a fuel additive is usually "added" to a fuel in small quantities, i.e 40 grams per 40 Kg of fuel.

Taylor et al[21] compared a mixture of fuel blends; they were blends of gasoline with several alcohols: ethanol, methanol, iso-propanol, and n-propanol. Emissions were reduced significantly, regardless of which alcohol used: carbon monoxide emissions were reduced by as much as 75%, hydrocarbon emission as much as 40%, and nitrogen oxide as much as 50%. However, Taylor et al did note that these reduction rates were very sensitive to fuel-air ratios.

Fleet testing using a mixture of butane-gasoline or butane-propane-gasoline was tested by Rodriquez et al[19]. They determined these mixtures did not affect the emissions very much. The increase in fuel economy was surprising; using a 50% mixture of butane and gasoline increased the fuel economy by 5%. This cannot be completely explained by the higher energy content of butane.

MTBE, or Methyl Tertiary Butyl Ether, has been used to reduce carbon monoxide, hydrocarbon, and nitrogen oxide emissions. This additive has been used for this reason for many years in most states as an oxygenate[9]. This particular fuel additive is made from by products of the oil refining process, and thus is relatively cheap to make; however this additive does not break down by natural processes and remains in the environment for a very long time if spilled. It is listed as a toxin and carcinogen, and can easily contaminate drinking water supplies. Once contaminated, water and MTBE are difficult to separate. For these reasons ethanol has mostly replaced MTBE as the

primary oxygenate[3].

1.2.2   Properties of Fuels

Determining the properties of fuels is an expensive process. It is also very time consuming, and for each property needed, a new test is required.

Pande and Hardy have developed a modified calculated carbon aromaticity index (CCAI) to calculate cetane directly from density and kinematic viscosity [17]. Pande and Hardy used the following equation: $CCAI = \rho - 81 - 141 \ln \ln(\nu + 0.85)$ with reasonable success (within 5% error).

Ichikawa et al. used proton nuclear magnetic resonance to determine the octane rating of several different fuels [10]. While the data seemed clear that the process does accurately work, the actual results must be taken lightly. The process calculates the amount of aromatics, olefins, and paraffins in the fuel mixture. From this and known typical properties of the fuel types one can accurately "guess" the octane rating. This method will fail if the fuel uses a fuel type which does not fall within one of the three categories used.

Another method to calculate octane rating, using FT-Raman Spectroscopy, is described by Cooper et al [5]. This method uses a similar approach as the previous method, it determines the percentage of aromatics and olefins in the fuel to estimate the octane rating. Cooper et al. acknowledges the limitations and uses a very large "training" set to compare against (208 samples) as a means to reduce the error.

A third method to calculate octane rating uses near-infrared absorption spectrum, by Korolev et al [13]. The method is significantly different from the previous two methods by using the absorption spectrum directly to calculate the octane rating rather than using the spectrum to compare against a large database of known fuels. This method is accurate (less than 1% error), however it is limited to fuels which are very similar to gasoline.

Cyclic variation and some properties were attempted to be determined using an absolute intensity method, known as characteristic vector sets, by Ippolito[11]. This method did analyze the cyclic variability of fuels quite well; however, the determination

of fuel properties was near impossible.

1.2.3   Spectroscopic Analysis

Spectroscopic Analysis of engines is difficult. The reason is simple, the environment of the engine is very harsh and does not lend itself to optical access. This being said, a few methods have been achieved.

Moeser and Hentschel used a fiber optic cable connected to a light pipe placed around the spark plug of the engine [16]. This method is one of the least intrusive methods for optical access. This method, however, does not allow for spatial imaging, only spectral. While this method does allow for the potential of minimum impact and species present in the combustion chamber, it does not allow for local species concentrations or flame front characteristics.

The Band-Ratio technique uses two infrared detectors to determine temperature and two species concentrations. This technique uses the integrated intensity across a vibration-rotational band of H_2O and CO_2. By using a ratio of integrated intensities, the band ratio does not need to have the black body curve vary significantly with temperature. This reduces the temperature errors associated with the band-ratio technique versus the two-color method[7].

The three-color method uses a modification to the band-ratio method. Use the band ratio temperature as a first guess. Iterate the extinction coefficient of water using the third band, which is primarily water vapor. Calculate the extinction coefficients of water from the other two bands, starting with soot as negligible; from those coefficients the emissivities can be calculated. The emissivities can be used to reduce the error of the the temperature calculation. This is continued until the change in temperature from one iteration to the next is less than some small error[4].

Starting with the two color method, then the band ratio, and finally the three color method, one may extrapolate more wavelengths, means better accuracy; this is true, however, there are difficulties. The four color method uses four cameras to determine: wall temperature, mixture temperature, water concentration, and soot concentration. The emissivity of the cylinder head must be determined previously by another method,

and may require a fifth camera. The actual calculation is, in theory, straight forward. Four equations, four unknowns; it is a simple system of equations problem[6].

While it seems simple, problems arise when considering error from the imaging devices, path lengths, environmental effects, etc. If these errors are considered, then multiple solutions to the system exist. These "other" solutions are sometimes significantly different. This actually leads to an acceptable fix; the solutions with temperatures wildly out of range of normal combustion can be neglected. More solutions can be neglected by assuming water is present in the combustion process, and in normal concentrations. This leads to a educated guess of the actual solution[14]. This process will only work if temperature and concentrations of the species in question have an expected range of valid answers, which is relatively small.

1.3 Present Work

The goal to study in-cylinder combustion reactions used many specialized apparatuses, including an optical access engine and high speed multi-spectral infrared cameras (Chapter 2). The optical engine needed to be redesigned based upon experiments previously performed [11] (Chapter 3). Digital circuitry was needed to be designed to ensure synchronous data recording (Chapter 4). A well-defined procedure is required to minimize the number of possible variables (Chapter 5). A novel robust statistical analysis method was developed to analyze the images from the cameras; qualitatively and comparatively (Chapter 6). The final objective is to prove the analysis tool's results are reasonable and useful. A blind test was performed using blended fuels from Afton Chemical and comparing their expected results to the results of the analysis (Chapter 7).

Chapter 2

Experimental Apparatus

The experimental apparatus consists of four major components: the engine, dynamometer, high speed infrared imagers, and the system control center.

2.1 Overview of the Apparatus

As described there are four major components of the apparatus. The engine and infrared radiation from the combustion gases is the primary focus of this investigation. The dynamometer controls engine RPM and thus controls loading applied to the engine. The high speed infrared imagers are aligned to the engine setup to receive the infrared radiation and record relative intensities. Finally, the system control center is a set of computers which controls the cameras and records all pertinent data (i.e. Infrared images, pressure-time data, etc).

2.2 Optical Access Internal Combustion Engine

The engine was modified to allow for optical access of the combustion chamber. This design allows infrared video to be recorded of the combustion as it occurs.

2.2.1 Stock Engine

The stock engine is a 1999 Ford 4.6L V8 engine. This engine was found in the late 1999 and early 2000 Mustang Cobra vehicles. Original specifications are displayed in Table 2.2.1.

Engine Model	Ford $281in^3$ (4.6L) V8 DOHC
Ignition Type	Distributor-less non-wasted spark
Fuel Delivery Method	Multi-port fuel injection (MPFI)
Number of Strokes per Cycle	4
Bore	$3.551in$ ($90.2mm$)
Stroke	$3.543in$ ($90mm$)
Connecting Rod Length	$5.96in$ ($151.5mm$)
Compression Ratio	$9.9:1$
Clearance Volume	$3.051in^3$ ($50cm^3$)
Number of Valves per Cylinder	4
Intake Valve Lift Intake Valve Diameter	$0.259in$ ($6.59mm$) $1.752in$ ($44.5mm$)
Exhaust Valve Lift Exhaust Valve Diameter	$0.259in$ ($6.59mm$) $1.338in$ ($34mm$)

Table 2.1: Engine Specifications [11][8][20]

2.2.2 Modified Engine

The engine was modified by Tarazi [20] to allow for optical access. This was accomplished by adding a second cylinder bank 7 inches above the left bank (the engine is set up with the rear of the engine outward and thus the visually right bank is the modified side in all pictures and diagrams) of cylinders. This setup is very similar to the Bowditch design.

An extended piston was then developed to be bolted onto the original piston. The extended piston has a large section of material removed from one side, which allows for the optical access. The top of the cylinder was replaced with a "window" of silicon. Such a "window" is quite opaque in the visible spectrum, however is rather transparent in the infrared spectrum, which is of interest. This extended piston has some technical issues that were solved with a redesigned version which will be discussed shortly. A stationary mirror was placed into the large cut out of the extended piston. This stationary mirror was then aligned with the high speed infrared imagers.

The modifications made to the engine were done to minimize the operating discrepancies between the modified engine and the original engine. A major modification which was done is that the engine now runs only on the extended piston (i.e. the other seven cylinders do not have moving pistons in them). This throws the rest of the engine off balance. To counteract this off balance-ness the crankshaft was balanced very carefully to minimize vibration on the system [20]. An air reservoir was added prior to the intake manifold to reduce fluctuations in the intake pressure because only one cylinder was working.

2.2.3   Issues with the Original Extended Piston (OEP)

The original extended piston (OEP) had some problems which needed to be resolved. These problems are all caused by a single fundamental flaw with the OEP. The OEP used five graphite compression rings instead of the OEM two iron rings. The use of graphite rings lets the OEP run with out lubrication, this works since the stationary mirror could become covered in oil. Unfortunately, the negative effects of the graphite rings far outweigh the positive effects.

The graphite rings have many problems: they do not seal as well as the iron rings, they wear quickly, and they do not center the piston as well. These three problems cause other problems. The worn graphite rings and the non-centering problem allow the OEP to make contact with the cylinder liner during engine operation. The worn graphite rings and the non-sealing problem encourage combustion gas blow-by. Both of these secondary problems cause the research data to become inaccurate after a short duration.

On one occasion the graphite rings wore quickly (15 minutes of run time) and then the piston rubbed against the cylinder liner, which effectively destroyed the cylinder liner (the OEP is stainless steel while the liner is cast iron). Figure 2.1 shows a comparison between a new and used graphite ring. The harsh environment of the engine usually cracks the graphite rings. It is not uncommon for some of the smaller pieces of the used graphite rings to become completely missing (it is assumed that these smaller pieces become stuck between the piston and the cylinder liner, and grind away).
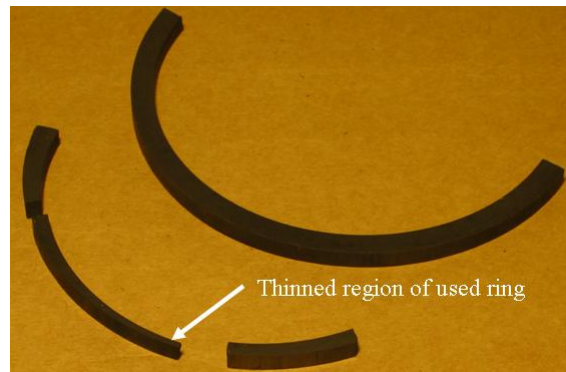
Figure 2.1: Used and New Graphite Rings

Continued abuse, such as overheating and physically scraping against the cylinder liner, resulting in the OEP starting to fail. Primarily the crown of the OEP started to warp in an irreparable way. Figure 2.2 is a closeup of the damage done to the piston. The warping is indiscernible, however, the vertical stria can be seen. This damage occurred when the piston rubbed against the cylinder liner. Thus, it seemed a new extended piston would have to be made.

Figure 2.2: Damage Done to OEP

2.2.4 Redesigned Extended Piston

The simplest solution to the OEP problems is to use the original iron rings from the stock piston and use a lubrication system. This solves the sealing problems, wear problems, and centering problems. It also cools the piston by increasing the surface contact the piston has with the coolant jacket (through the oil). Unfortunately, this simple solution is not a perfect solution. Since oil must lubricate the REP, a method to add and remove the oil must be designed. The systematic design of the REP is discussed further in chapter 3.

2.2.5 Pressure Sensor Location

Up to this point, no mention of where or how the pressure transducer is located has been made, however it seems pertinent to explain where it is. The pressure sensor was recently moved from a spark plug pressure tap to a spot located within the cylinder head. The location on the spark plug works because it requires no modification to the head, however, it does require a special spark plug to be made. In this position, the pressure sensor would be inaccurate due to the damping from the long thin tube required. Also, interference from the spark plug is noticeable.

The new location on the cylinder head is located within a structural aluminum rib between the combustion chamber and the external part of the head. The inside of the rib was drilled out and reinforced with steel to house the pressure sensor. A small pressure tap $3/32in$ in diameter by $1/8in$ deep was placed in between the combustion chamber and the pressure transducer.

2.2.6 Oxygen Sensor

The oxygen sensor for this engine was originally a wide-band O^2 sensor, however, the sensor equipment started failing prior to data collection. The decision to replace the wide-band sensor with a narrow-band sensor was made for two reasons. First, a narrow-band sensor is significantly cheaper, and second, it is a more accurate means of measuring stoichiometric combustion. The narrow-band sensor indicates above, below,

or at stoichiometric combustion conditions, while the wide-band sensor also indicates how "off" from stoichiometric the combustion is. The electronics needed to run the narrow-band is simple: power is required for the heating system inside the sensor, and a high-frequency filter is required to be placed on the signal out from the oxygen sensor. The high-frequency filter is a misnomer, because the filter is set to block signal above 10Hertz. This signal is then sent to a multimeter to read out the voltage level. Above 0.9V is rich running, below 0.1V is lean running, and between 0.1V and 0.9V is very near stoichiometric (within 1% error).

2.3   Dynamometer

The dynamometer consists of a 40HP DC General Electric electric motor and a controller. The dynamometer has two operating modes: RPM select and torque select. In the first mode, a rotating speed is selected in RPM, which is then held constant. In the second mode, a torque is set and the motor consistently applies that torque, regardless of RPM.
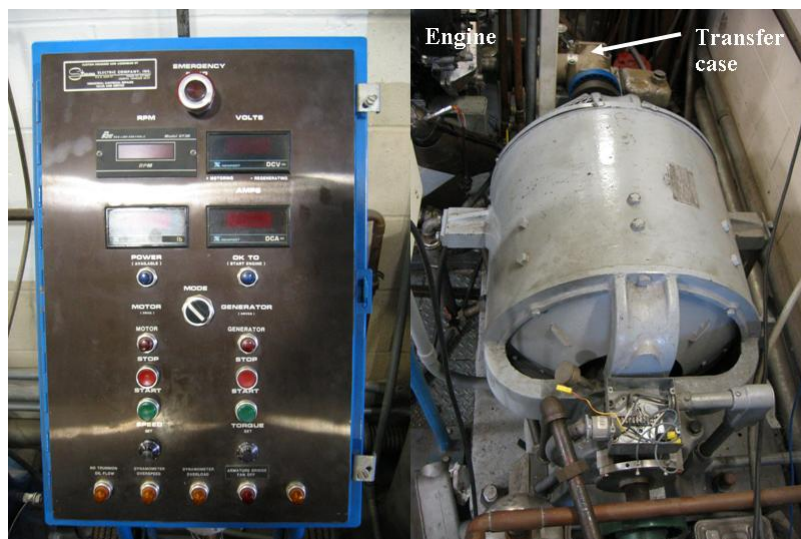
Figure 2.3: Left: Dynamometer Controller. Right 40HP General Electric DC Dynamometer

On the left of Figure 2.3 is a figure of the dynamometer controller custom-built for Rutgers University by Stevens Electric Company. On the right of Figure 2.3 is a figure of

the actual dynamometer connected to the engine. At the top of this figure is a transfer case (gold housing above blue ring), which redirects the power of the dynamometer to the engine.

2.4   High Speed Infrared Imagers

The Rutgers Super Imaging System (SIS) is an advanced infrared imaging device. This device is the culmination of many years worth of dedication by many individuals, most notably Mārcis Jansons [12] for the physical devices and Shu Lin [14] for the systems control software.

SIS consists of five platinum-silicide (Pt-Si) CCD cameras. Four of the five cameras are set up such that the optical path to each of the four cameras are identical. Figure 2.4 is a layout of the spatial cameras. There are three radiation splitters, ranges of which are chosen specifically to direct appropriate wavelengths toward the appropriate camera. Each camera then has a narrow band filter placed in front to filter out any unwanted radiation directed towards it by the beam splitters. The filters are centered around 2.1, 2.47, 3.42, and $3.8\mu m$.

The four spatial cameras are capable of producing 62 images during the combustion processes, of consecutive cycles. This is important for the study of cyclic variations

The last camera is dedicated to a modified Fastie-Ebert Spectrometer [12]. The spectrometer was not used in the experiment, and thus, it will not be further discussed; it is here only for completeness.

2.5   System Control Center

The system control center is comprised of several individual systems. These systems interface with the engine and the imagers which results in a more compact control center which can be run by an individual with relative ease. The control center is shown in Figure 2.5. This system uses two IBM compatible PC's, a Rutgers University built fuel controller, a digital multi-meter and an oscilloscope (not shown).

The lower of the two PC's (labeled as Imaging PC in Figure 2.5) controls the
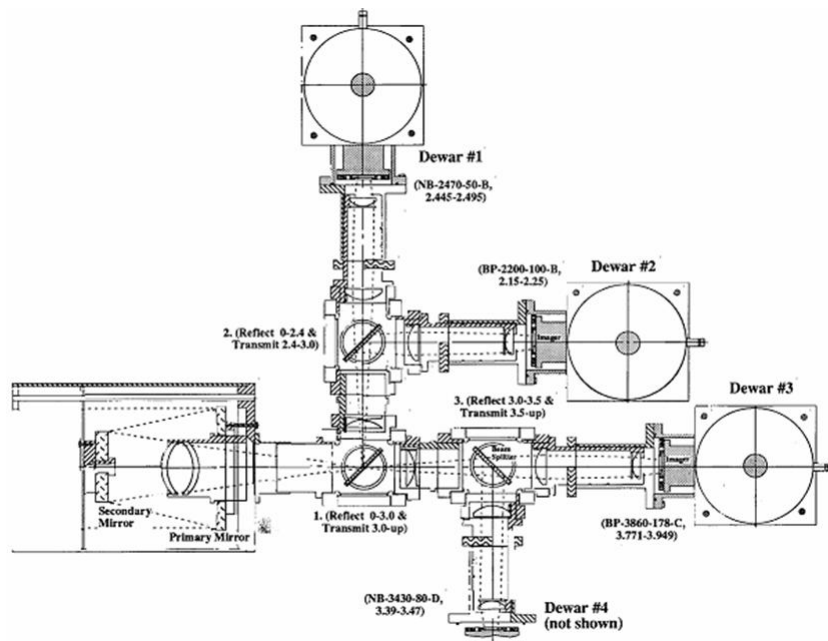
Figure 2.4: Spatial Camera Layout
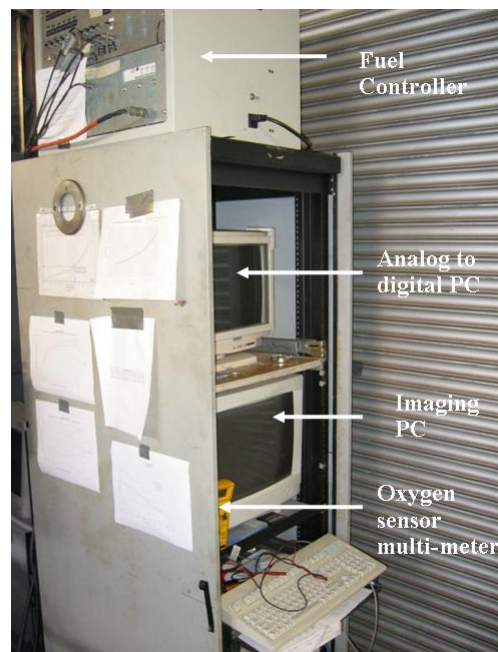
Figure 2.5: System Control Center

high speed infrared imagers. This PC contains the application RAP, short for Rutgers Animation Program. This application is the heart of the camera controlling software, which was designed at Rutgers primarily by Shu Lin [14]. This PC records the 62 frames of consecutive combustion cycles of the engine. The number of consecutive cycles capable of being recorded is limited only by the available disk space.

The upper PC (labeled Analog to digital PC in Figure 2.5) records up to 12 analog pulses every half crank angle. The three important analog signals are cylinder pressure, fuel/air ratio, and fuel pulse timing. A second computer is required to handle the analog to digital conversion because the band-width of the PCI interface of a computer is not capable of handling both the imaging data and the analog data.

The multi-meter (labeled Oxygen sensor multi-meter in Figure 2.5) allows for real time fine tuning of the fuel flow. This allows for very near stoichiometric combustion.

The oscilloscope shows the real time pressure time data of the engine. This is useful in determining the health of the engine, and possible hazards before they develop into larger problems.

Chapter 3

Redesigned Optical Access Engine

As described in section 2.2.3 there are severe limiting issues with the original extended piston (OEP). In this chapter a detailed analysis and steps to solve these issues will be described.

3.1   Designing an Extended Piston

The biggest design constraint is the engine itself. This means that the overall outside diameter (OD) cannot be any larger than the bore $(3.551in)$ of the engine. However, with clearance spacing around the piston $(.0125in)$ the diameter of the piston becomes a fixed value of $3.525in$. The clearance value was set by Ford Motor Company or the OEM, thus, the new piston diameter will be the exact diameter of the OEM piston [8].

The next design constraint is the window which replaces the piston crown. To maximize the viewing area, the largest window possible is selected. The window with the best possible infrared transmissivity is sapphire or silicon[1]. Unfortunately, the sapphire and silicon are both quite brittle. A protective stainless steel shell must be placed around the window to ensure the window stays in static equilibrium with respect to the rest of the piston. A window diameter selected as a function of the protective shell and the OD is $3in$.

Another constraint is the stationary elliptical first surface mirror. The mirror is angled at $45°$ inside the extended piston, and must remain untouched while the engine is running. A hole, measuring at least $3in$ wide, must be placed int the side of the piston. The height is determined by the stroke plus the overall height of the mirror

---

[1]Sapphire has a better transmissivity; however it is more brittle. Thus silicon is also used as it handles the abusive environment of an engine better.

assembly. With a small safety factor the height was selected to be $7.30in$.

Another constraint is that the new piston must weigh very closely to the weight of the previous design. Otherwise the engine would need to be completely rebalanced, a costly and time consuming task. Unlike the previous design a second, smaller hole was to be cut out of the side of the piston. This hole is exactly opposite from the primary hole. The purpose of the hole is to move the center of mass closer to the geometric center of the piston in an attempt to reduce the tendency of the piston to wobble. This also reduced the overall mass of the piston to be closer to that of the OEP. The new piston is approximately $2oz$ ($56.7g$) heavier, which is not enough to dramatically affect the balance of the engine.

Figure A.6 is a three-dimensional figure of the REP from PRO/E. Figure A.7 shows an exploded view of a simplified piston assembly. Figure A.8 is a mechanical drawing of the REP with dimensions.

The entire assembly was redesigned and fabricated during the course of the present study. As explained more below, it includes new specialty tools developed for successful component fabrication.

3.2   Redesigned Extended Piston Version 2

During calibration and simple testing of the REP, a catastrophic failure of a weld occurred. Many factors contributed to the failure: stainless steel generally becomes brittle near a weld, welding two different metals is difficult, the weld surface area is small, etc... The second piston that had to be made is from a single piece of 316 stainless steel. Other than the single piece of metal, the two pistons are identical in shape. Thus, the first REP will not be discussed further.

3.3   Fabricating a Piston from Raw Material

To build an extended piston from steel is an enormous task. A typical machine shop would require two months to complete the task, and would cost a total of $6000(est.). A machine shop would also require complete and detailed drawings of the entire piston.

The piston was built over seven months within the Mechanical and Aerospace Engineering Machine Shop at Rutgers University. The machine shop while capable, does not have the specialty tools which are needed to fabricate something as complicated as the REP. Some specialty tools, such as the two grooving tools required for the ring grooves, were bought since they are cheap and readily available. Unfortunately, some of the more specialized tools are difficult or impossible to find a retailer for.

3.3.1 Boring Bar Holding Fixture

A boring bar is used to cut the inside of a mechanical tube while working on the lathe. The boring bar is essentially a long solid round stock of steel with a specially shaped hole on one end to hold lathe tool bits. Unfortunately, a boring bar's shape does not lend itself to being held without a special fixture. That is where the boring bar holding fixture comes in. The fixture is a large block of aluminum designed to hold a 1.125in
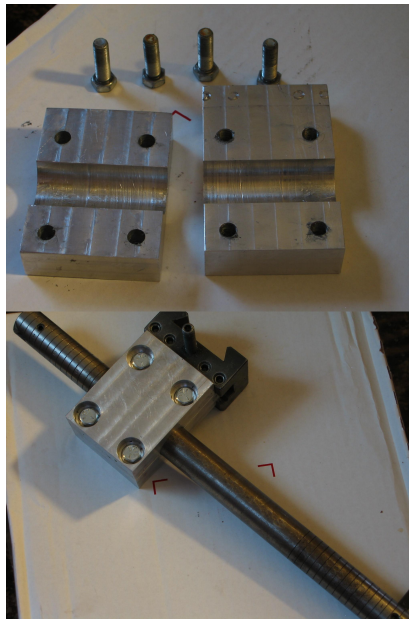

Figure 3.1: Boring Bar Holding fixture. Top: Exploded. Bottom:Assembled.

boring bar. Smaller diameter boring bars could not have been used due to the depth of the boring (up to 7in) and strength of the material to be cut, stainless steel. The original boring bar holding fixture was misplaced and as a result a new one needed to

be made.

3.3.2 Rolling Steady Rest

A steady rest is used to stabilize a long rotating part on a lathe. This is accomplished by forcing three contacts against the rotating piece. These contacts hold the axis of the part fixed relative to the head stock axis. This was actually modified from a brass tipped steady rest. There were two problems with the brass tips: heat and size. The hot-working temperature for brass is $1400°F - 1600°F$. During cutting of steel, in which a significant amount of material needs to be removed, the steel becomes a blood red[2]. This temperature, the pressure, and the friction between the brass and the steel can easily deform the brass. The tips were also too large and would not allow for a large diameter piece to be placed with it. The modified steady rest used shorter tips,

Figure 3.2: Steady Rest Inserts Original (Left) and Modified (Right).

which had small stainless steel ball bearing rollers fitted. Figure 3.2 is a picture of a brass tip (left) and new tip with bearing (right). The two pictures are of similar scale for visual reference to size. The adjustment screw is visible in the right figure.

---

[2]Blood Red is a steel working term for the "heat colors of steel" which corresponds to approximately $1050°F$ [2]

3.3.3   3.100in Internally Expanding Collet

A collet is a specialized tool designed to grab a specific diameter round cylinder. It may either grab by constricting concentrically around the cylinder or concentrically expand around the inside of the cylinder; this tool is of the latter type. A specialized collet needed to be made. The few collets which are 3.1in in diameter were not designed to handle the high rotating inertia. The collet was designed to maximize the holding surface area[3], which is $22.6in^2$! This large holding area allowed for the primary method for holding the REP during most of its fabrication. Figure 3.3 is a picture of the new collet made; on the right is an NPT pipe plug. The slightly tapered nature of the NPT threads forces the four wedges apart as the plug is threaded into the collet.
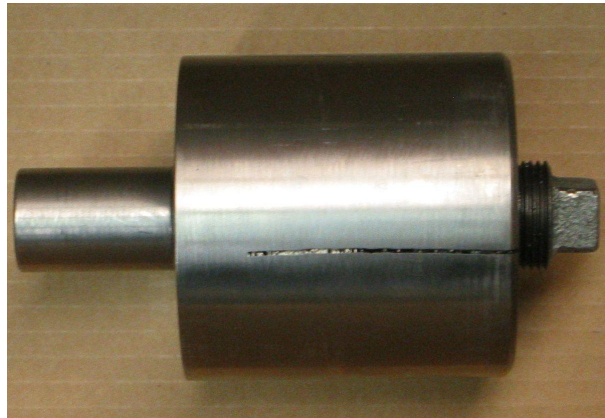
Figure 3.3: 3.100in Internally Expanding Collet

3.3.4   Vertical Angle Indicator and Hold-Down Fixture

The vertical angle indicator is a setup which shows the rotary angle the piston is set at, relative to some fixed position on the piston. The hold-down fixture, as its name implies is used to hold down the piston; however with minor adjustment it allows for rotation of the piston. The vertical angle indicator and the hold-down fixture work in

---

[3]The holding surface area of an internally expanding collet is not the entire external surface. The collet grabs by deforming the large plates outward. This particular collet was made so a large percentage (about 75%) of the surface comes into contact with the REP simultaneously. This was accomplished by slightly tapering the collet.

conjunction to allow the odd angles needed for the back of the REP.

Figure 3.4: Vertical angle indicator and hold-down fixture

Figure 3.4 is a picture of the vertical angle indicator setup and the hold-down fixture; from left to right: bottom hold down bracket, top hold down bracket, digital protractor support, and digital protractor. The first two are used with long bolts and t-nuts to hold the piston to the bed of a milling machine. The support is to hold the digital protractor at 90° to the REP. The digital protractor is then used to indicate the angle at which the piston is placed at, and can be read off the LCD screen.

3.3.5   Fabricating the REP

The REP started as a 24in long 4in OD and 2.5in ID 316 stainless steel mechanical tubing.

The tube was first held externally while the bottom was machined to the finished $3.1in$ diameter and the threading was cut, figure A.2. This allowed the use of the $3.1in$ collet allowing for a continuous and concentric machining of the critical piston crown, inside and out, figure A.3. There are two sets of threading on the REP; one set is a reverse threaded 16 threads per inch, used for the window locking nut. The other is a

standard 20 threads per inch used to mount the REP to bottom piston via the bottom plate. The final step is to cut the two large holes in the piston. The finished piston and its pieces may be found in figure A.4. A spanner wrench was designed to allow the locking ring to be tightened and loosened with relative ease; this is shown in figure A.5.

3.4   Oiling Mechanism

Since the OEP used graphite compression rings, no oil was needed. However, the REP is designed with stock steel rings and thus requires oil. Unfortunately, using the stock oiling system was out of the question since an oil film free mirror must be placed inside the REP. A simple solution was to use a gravity fed oil drip mechanism which feeds oil through the water jacket around the cylinder. The sealing mechanism and tubing for the oil through the cylinder block is shown in figure 3.5.
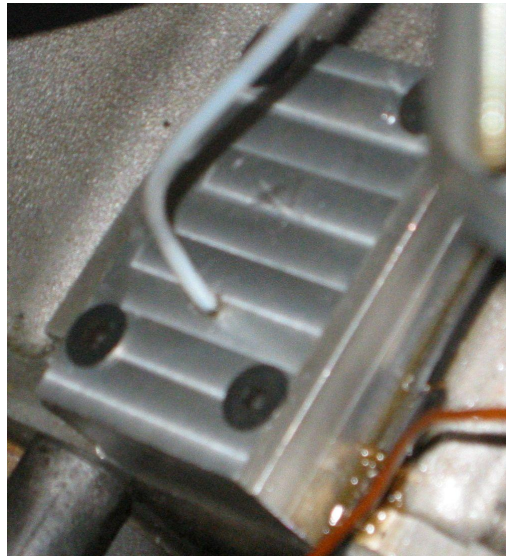
Figure 3.5: Oil feed for the REP

3.5   Six Degree of Freedom Mirror Fixture

The original mirror fixture which was used with the OEP did not allow for much adjustment. This fixture needs many degrees of freedom since it is difficult to manipulate

the camera system in three-dimensions. This may, at first, seem a moot issue, but the mirror must reflect the infrared radiation directly towards the Cassegrain collector of the camera system. This means that each of the 6 degrees of freedom for both the camera and the mirror must be aligned properly. The six degrees of freedom are the X, Y, Z directions plus the rotations about said axes.

Figure 3.6: New mirror mount

Chapter 4

Digital Timing Circuit

In implementing the present study, the digital timing circuit for the data collection system, including the camera system, needed to be replaced. The timing circuit controls the synchronization of all five cameras, the computer system, and the analog to digital data converter. Unfortunately, the original circuit diagrams did not exist, nor did the program for the complex programmable logic device (CPLD). The design of the new circuit board was based upon two things: what was known to be passed into the circuit, and what was expected of the circuit to do.
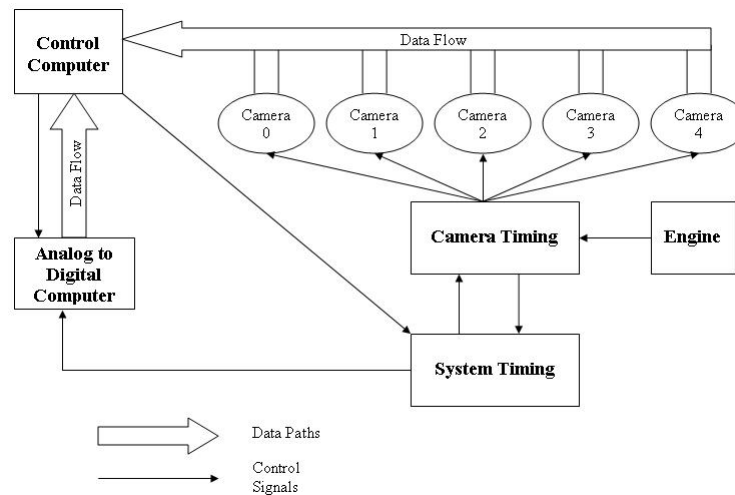

Figure 4.1: Camera System Layout

Control information is sent to the system synchronization board via a parallel port from the control computer. Synchronization signals from the engine encoder get sent through the camera synchronization board via a 14 conductor ribbon cable. Synchronization signals are then sent to the camera synchronization board and to the analog

to digital computer.

Pin Number	Pin Name	Description	Active
1	Data 4	Control Signal	not active
2	Data 2	Control Signal	not active
3	Address 2	Control Location	not active
4	Address 4	Control Location	not active
5	Crank Angle In	CA Engine Synchronization	Active
6	Strobe 4	Control Response	not active
7	Strobe 2	Control Response	not active
8	Data 3	Control Signal	not active
9	Data 1	Control Signal	not active
10	Address 1	Control Location	not active
11	Address 3	Control Location	not active
12	TDC In	TDC Engine Synchronization	Active
13	Strobe 3	Control Response	not active
14	Strobe 1	Control Response	not active

Table 4.1: Input from Camera ribbon cable connector

During the redesign, most of the signals from the other synchronization card where discarded, as shown in table 4.1. The two signals which are used from the other synchronization circuit are the TDC and CA synchronization signals. These signals are then passed through an inverting line driver to the Altera CPLD chip.

The parallel port is connected to the circuit via a 26 conductor ribbon cable; the pin out is described in table 4.2. The signals labeled with a (-) are active low signals, in other words, the digital signal on the pin is high and turns low when a signal is sent. An output parallel signal is boosted using two 8-way non-inverting tri-state line drivers, 74F244N.

The output signal to the analog to digital computer is output via 3 3 pin headers. The first of which outputs crank angle and top dead center signals. The second outputs analog to digital trigger only. The third outputs simulated crank angle and simulated

Pin Number	Pin Name	Description
1	-Strobe	Control Select
2	Data 0	Address Bit 0
3	Data 1	Address Bit 1
4	Data 2	Address Bit 2
5	Data 3	Address Bit 3
6	Data 4	Data Bit 0
7	Data 5	Data Bit 1
8	Data 6	Data Bit 2
9	Data 7	Data Bit 3
10	-Ack	Not Used
11	Busy	Not Used
12	PE	Not Used
13	-SLCTD	Not Used
14	-AutoFDXT	Control Select
15	-Error	Not Used
16	-Init	Control Select
17	-SLCTIN	Not Used
$18 - 26$	Ground	

Table 4.2: In From Computer ribbon cable connector

top dead center signals. The large 99 pin board edge connector is used only to supply power from the back plane bus of the system.

Pictures of the circuit board and its etch resist layout mask are depicted in figures C.1, C.2, C.3, and C.4.

All of the signals processing is done via Altera's CPLD, MAX-EPM7128SLC84-10. MAX being the chip type. The 7 indicating it is a 7000 series chip. The 128 indicating it has 128 macrocells (level of complexity). The S indicating the chip runs on 5.0 Volts. LC84 indicates it is of the PLC socket design, with 84 pins. The 10 indicates it has a response time of 10 nanoseconds. With this chip, Altera has packaged a simple "circuit" based design suite, in which virtual circuits are programmed onto the chip, called Quartus 2.

The program installed onto the CPLD can be seen in figure 4.2. There is an oddity with Quartus 2; it does not allow renaming of "test" pins, i.e. outputs from circuits which do not actually have a physical output cannot be renamed. This explains why some of the output structures have names similar to "pin_name3". While the CPLD is connected to a computer these outputs may be virtually tested rather than using a physical testing device.

There are two classifications of commands which are used by the camera system: Control and Property. Control commands are used to put the system in a temporary mode; not dissimilar for a keyboard's control or alternate keys. All control commands are distinquished by the strobe signal changing state from low to high. Property commands are usually used to set properties such as "number of data samples". All property commands are distinquished by the init signal changing state from low to high.

For this circuit, all property commands must be preceeded by the "Access PLA Addresses" control command. This is the only control command needed for this circuit. Other control commands are used for setting system operation mode, phase state, individual camera properties, etc... The "Access PLA Addresses" command is shown in table 4. Where the D# indicates a data signal and the A# indicates a address signal from the parallel port.

Most of the property commands set a $12 - bit$ unsigned binary integer for a specified
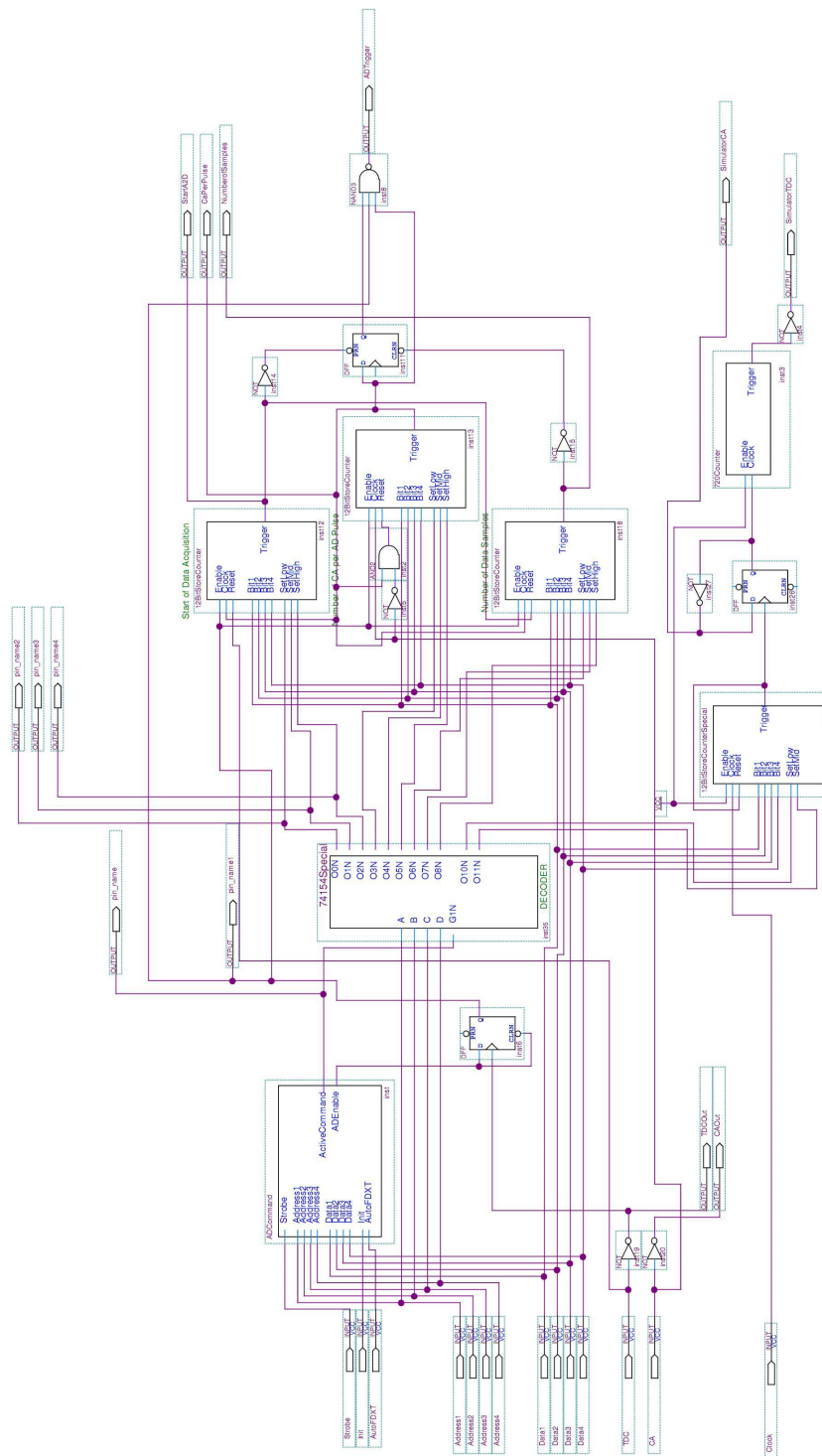
Figure 4.2: CPLD Main Program

Command	D4	D3	D2	D1	A4	A3	A2	A1	Strobe	Init
Access PLA Addresses	0	0	0	1	1	1	1	1	$0 \rightarrow 1$	NA

Table 4.3: Control command[12]

property. Since there are only 4 data signals, 4 bits are set at a time. Thus it requires 3 separate property commands to change a value. The properties are: encoder pulses per AD pulse, start of aquisition, number of data samples, and simulation counter. These commands are shown in table 4; where the B# represents the associated bit for that property.

Command	Nybble	D4	D3	D2	D1	A4	A3	A2	A1	Strobe	Init
Start of	Lower	B3	B2	B1	B0	0	0	0	0	NA	$0 \rightarrow 1$
Acquisition	Middle	B7	B6	B5	B4	0	0	0	1	NA	$0 \rightarrow 1$
	Upper	B11	B10	B9	B8	0	0	1	0	NA	$0 \rightarrow 1$
Encoder	Lower	B3	B2	B1	B0	0	0	1	1	NA	$0 \rightarrow 1$
Pulses per	Middle	B7	B6	B5	B4	0	1	0	0	NA	$0 \rightarrow 1$
AD Pulse	Upper	B11	B10	B9	B8	0	1	0	1	NA	$0 \rightarrow 1$
No. of	Lower	B3	B2	B1	B0	0	1	1	0	NA	$0 \rightarrow 1$
Data	Middle	B7	B6	B5	B4	0	1	1	1	NA	$0 \rightarrow 1$
Samples	Upper	B11	B10	B9	B8	1	0	0	0	NA	$0 \rightarrow 1$
Simulation	Lower	B3	B2	B1	B0	1	0	1	0	NA	$0 \rightarrow 1$
Counter	Middle	B7	B6	B5	B4	1	0	1	1	NA	$0 \rightarrow 1$
	Upper	B11	B10	B9	B8	1	1	0	0	NA	$0 \rightarrow 1$

Table 4.4: Properties commands[12]

There are two commands which are classified as property commands, however, they do not actually set properties: activate AD pulses and deactivate AD pulses. Their use is self explanatory, but they require a series of signals sent to be activated, which are described in table 4.

The program is easily broken in to a few sections. Starting in the upper-left of figure 4.2, the object labeled ADCommand handles the "Access PLA Addresses", "Activate AD Pulses", and "Deactivate AD Pulses". The object ADCommand has its own

Command	D4	D3	D2	D1	A4	A3	A2	A1	Strobe	Init
Activate AD	0	0	0	0	1	0	0	1	NA	$0 \to 1$
Pulses	0	0	0	1	0	1	0	0	NA	NA
Deactivate	0	0	0	0	1	0	0	1	NA	$0 \to 1$
AD Pulses	0	0	0	0	0	0	1	0	NA	$0 \to 1$
	0	0	1	0	1	0	0	1	NA	$0 \to 1$

Table 4.5: Activate/Deactivate commands[12]

program associated with it, shown in figure C.12.

The object labeled 74154Special, near the middle, is a simple decoder which interprets the property commands and sets the appropriate 4-bit nybble. Each 12-bit number is stored in its respective 12BitStoreCounter or 12BitStoreCounterSpecial. The 12BitStoreCounterSpecial is identical to a 12BitStoreCounter, except the high 4-bit nybble was removed to reduce storage space (technically it is now an 8-bit store counter). The 12BitStoreCounters are responsible for outputting the proper sequence of triggers for the analog to digital board.

The lower-right region, consisting of the 720Counter and the 12BitStoreCounterSpecial, is special coding designed to simulate the responses from an engine while it is running. This allows analysis and debugging of the complex camera system without having the engine running.

A complete list of the program is found in Appendix C.1.

Chapter 5

Experimental Procedure

Previous research has lead to an understanding of how SIS responds to situational parameters. Much effort has gone in to removing every variable that is possible to control, which should give repeatable results.

Previous research has required many hours of preparatory work to set up the experimental apparatus. Setup would include: Cooling of camera system, aligning the optical tube, aligning the mirror assembly, cleaning the silicon window, preheating the engine, verifing the functionality of all electronics, etc... This would lead to a very cumbersome problem of achieving a maximum of two experiments per day. The current research however has 62 experimental data sets. Considering that not every day is feasible to run the experiment (due to climate in the laboratory), it would take several months to complete.

New locking mechanisms were made to stabilize and prohibit the motion of the camera system. A new mirror carriage assembly was made to make daily alignment unneeded. A mirror cover was created by rapid prototype to protect the mirror when it was not being used. A new vacuum system was put into place to slow the warming of the camera system. All of these new mechanisms and devices allow for more repeatable experiments.

Initially the camera system was aligned very accurately with the mirror assembly, and all of the moving pieces were locked into place. This was done only once, keeping the alignment the same from experiment to experiment. The engine was also initially preheated to the $\sim 75°C$ required, and kept at that temperature for the duration of the experiments. Table 5 is a list of the constant system parameters.

Engine Speed	600rpm
Coolant Temperature	$\sim 75°C$
Intake Manifold Pressure	-5 inHg
Spark Timing	$6°$ bTDC
Fuel Injection Timing	$120°$ aTDC
Run Time on Propane	1.5 minutes
Run Time on Fuel	1 minute

Table 5.1: Constant Parameters

Every morning the camera system would require an initial cool down of liquid nitrogen (LN_2); this would consume about 2 liters of LN_2.

The experimental procedure is as follows:

1. *Verify the camera system is cold enough to properly run, fill dewars with LN_2, as necessary.*

2. *Clean mirror throughly with optical cleaner and replace cover.*

3. *Remove window assembly, clean all parts with acetone, clean all parts with optical cleaner, and blow dry with compressed air. (Done every other experiment to see the effects of soot build up)*

4. *Replace window assembly using vacuum grease to hold gasket in place between the silicon and spacer ring.*

5. *Ensure the fuel pump, spark system, and 0_2 Sensor are on.*

6. *Record environment parameters (absolute pressure, air temperature and relative humidity).*

7. *Start dynamometer and set to 600 RPM.*

8. *Initialize camera system ensuring it is in the right phase, switching to proper phase if not.*

9. Start fuel injection, adjust fuel flow as required to achieve stoichiometric combustion.

10. Run for 2 minutes.

11. Record background radiation.

12. Remove camera cover and mirror cover.

13. Start Recording of data (100 cycles).

14. Stop fuel injection, fuel pump, spark system, and dynamometer.

15. Convert mil Files to im files. Verify the collected images are what was expected. No obvious defects visually apparent, typically caused by failure of the window seal or excessive oil buildup on the mirror or window.

16. If images pass then change fuel, otherwise redo the experiment.

Changing the fuel is a process in itself.

1. Turn on fuel pump.

2. Open the high pressure drain valve, low pressure drain valve, and the fuel fill hole. Draining fuel into a hazardous waste container.

3. Let fuel drain completely. Close high pressure and low pressure drain valves.

4. Refill tank with new fuel. Let run through fuel system for 5 minutes.

5. Again open the high pressure drain valve, forcibly cleaning the high pressure side of any residual previous fuel.

6. Once the high pressure runs dry open the low pressure drain valve.

7. Once both drain tubes are completely empty, close both valves.

8. Refill tank with new fuel again.

9. Close tank fill hole.

Chapter 6

Computer Assisted Statistical Analysis Tool (CASAT)

The Computer Assisted Statistical Analysis Tool (CASAT) consists of a set of robust statistical analysis tools combined with more advanced techniques developed specifically for analyzing infrared images generated by using the Rutgers Super Imaging System (SIS).

6.1 Mathematical Nomenclature

To continue, some mathematical ground work needs to be described. For the following discussion time is broken into two variables t and c. The first representing crank angle measured from top dead center of the combustion stroke of a particular cycle, and the latter representing cycle number starting from the start of recorded data. Thus $F^{t,c}$ represents an intensity at a particular cycle and crank angle.

For spatial analysis, (x_i, y_i) is used to indicate the coordinates of a particular pixel i, with the upper left corner of the image being $(0, 0)$ and the lower right being $(63, 63)$. $F_{x_i,y_i}^{t,c}$ identifies the intensity of the particular pixel i at the crank angle t, and cycle c. For ease of reading $F_{x_i,y_i}^{t,c}$ will be simplified to $F_i^{t,c}$.

6.2 Robust Statistics

Robust statistics is an offshoot of statistics in which data is not affected by data outliers, or at least minimizes the effects of data outliers. Many robust methods exist and are well documented in statistics text books such as Robust Statistics by Maronna[15]. The robust statistics methods used were specifically chosen for the range of "robustness" and for the computational speed in which they are calculated. The reason for multiple

algorithms is occassionally an algorithm is too robust, which results in important information being lost. Table 6.1 is a list of location estimates used, most well known is mean or average.

Consider a numerical set $\bar{x}$ which is sorted, smallest numerical value first. N is the total number of values within the set $\bar{x}$.

Location Estimate	Robustness	Equation
Mean	None	$mean(\bar{x}) = \frac{1}{N} \sum_{j=1}^{N} [\bar{x}_j]$
Median	High	$med(\bar{x}) = \frac{\bar{x}_{m+1} + \bar{x}_m}{2}$
α Trimmed Mean	Very High	$atm(\bar{x}) = \frac{1}{N-2k} \sum_{j=k}^{N-k} [\bar{x}_j]$

Table 6.1: Robust Location Estimates [15]

where $\quad m = \frac{N+1}{2}$ if N is Odd

$\qquad m = \frac{N}{2}$ if N is Even

$\qquad k = \alpha N$

$\qquad 0 \leq \alpha \leq 0.25$

For this entire document $\alpha = 0.25$.

Table 6.2 is a list of scale estimates used, most well known is the standard deviation.

Scale Estimate	Robustness	Equation
Standard Deviation	None	$stddev(\bar{x}) = \sqrt{\frac{1}{N-1} \sum_{j=1}^{N} (\bar{x}_j - mean(\bar{x}))}$
Median Absolute Deviation (MADN)	High	$madn(\bar{x}) = \frac{1}{0.6745} med\{|\bar{x} - med(\bar{x})|\}$
α Trimmed Standard Deviation	Very High	$atsd(\bar{x}) = \sqrt{\frac{1}{N-2k} \sum_{j=k}^{N-k} (\bar{x}_j - atm(\bar{x}))}$
Interquartile Range (IRQN)	High	$irqn(\bar{x}) = |\bar{x}_{N-k} - \bar{x}_k|$
Range	Low	$range(\bar{x}) = |\bar{x}_N - \bar{x}_1|$

Table 6.2: Robust Scale Estimates [15]

6.3   Characteristic Vector Sets (CVS)

The Characteristic Vector Sets method (CVS) was originally described in Lin's [14] work; and again by Ippolito [11]. However, a brief overview will be supplied here for completeness.

CVS selects the top x percent of the most intense pixels located in each image (where x is near 10, however this may be varied). These selected pixels are then grouped together for each frame of every cycle. A characteristic vector is then created for each of these groups.

A characteristic vector is defined as follows

$$\vec{V_A} = \frac{\int \int_A F_{x,y} \left(x\hat{i} + y\hat{j} \right) dxdy}{\int \int_A dxdy} \tag{6.1}$$

Where A is the area consisting of all pixels located in a specific group. A maximum number of characteristic vectors per frame is usually three; however this may be varied.

The characteristic vectors across cycles are grouped together; similar to the grouping previously described. Characteristic vectors are calculated for the grouped characteristic vectors, which in turn, is called a characteristic vector set. Two stability factors can then be calculated from the characteristic vector sets.

The geometric stability factor is calculated as follows

$$SF_D = \frac{N}{c_m}\sigma_d \tag{6.2}$$

Where c_m is the number of cycles contributing to the stability factor. σ_d is the standard deviation of the Euclidean distance from the mean characteristic vector set. The intensity stability factor is calculated as follows

$$SF_I = \frac{N}{c_m}\frac{\sigma_I}{E} \tag{6.3}$$

Where σ_I is the standard deviation from the intensity of the mean characteristic vector set. E is the intensity of the mean characteristic vector.

The stability factors are a quick method to determine the stability of a fuel. Unfortunately, the stability factors, while useful, are prone to significant errors. The problem

arises in how the pixels are selected. The maximum x percent of the frame may change rapidly from frame to frame. This method of selecting pixels also experience problems if there is a hot spot within the engine. This is not a characteristic of the fuel, but of the engine itself. Thus, the "characteristic vector" will not accurately predict how this fuel will work in another engine. Many of these problems are addressed and solved with the time derivative spatial averaging method.

6.4   Time Derivative Spatial Averaging (TDSA)

The Time Derivative Spatial Averaging (TDSA) uses a relative approach to analyze the infrared images, as opposed to the absolute method used in the CVS method. This allows the largest changes from crank angle to crank angle to be easily recognized. Unlike in the CVS method, however, using the top 10% of each image is not a satisfactory method; All pixels are required to make any meaningful observations of the data.

A background radiation image is used to reduce background noise, however this does not affect time varying biases in individual pixels. TDSA uses the previous image in the form of the time derivative to reduce this error.

The first step of the TDSA procedure is to find the time derivative of all the pixels of every frame and cycle. This is calculated by:

$$\frac{dF}{dt}\bigg|_i^{t,c} = \frac{F_i^{t+1,c} - F_i^{t,c}}{T} \tag{6.4}$$

Where T is the time between each frame, which is $5.55 \times 10^{-4} s/frame$. Then the average time rate of change of intensity is calculated by applying equation for mean location estimate from section 6.2 to equation 6.4.

$$\frac{dF}{dt}\bigg|^{t,c} = mean\left(\frac{dF}{dt}\bigg|_i^{t,c}\right) \tag{6.5}$$

Location and scale estimates are then calculated against equation 6.5 across cycles. The location estimates result in cyclic "averages", while the scale estimates result in cyclic variances. The location estimates are then used to make qualitative comparisons about various fuels, further discussion in chapter 7.

6.5   Flame Front Tracking

Another process based upon the time differential is qualitative flame front comparison; start with equation 6.4 and then select the largest 10% of the pixels. These are then geometrically grouped together using a simple recursive algorithm. The largest group is then plotted to show the flame front propagation. It is realized that this method is not the most ideal method for determining the "motion" of the flame front, however, due to the high speed nature of combustion and the relatively low temporal and spatial resolution of the camera system, a more accurate method is not achieveable.

6.6   CASAT the Application

The application was written in Microsoft Visual Studio .Net C# version 2.0. This programming language was chosen as it is based around the idea of Rapid Application Development (RAD). The applications developed with C#, are generally less computationally expensive than with the more traditional languages such as C++. The reason for this quicker execution time is from the libraries designed for the .Net framework. Many of the simple libraries, which normally a C++ programmer supplies, are highly optimized pieces of code developed by Microsoft.

6.6.1   The Graphical User Interface (GUI)

An application was developed to use the CASAT library. This application entitled Rutgers Imaging Application (RIA for short), is a simple utility which allows access to the functions of the CASAT library.

Pictures of the GUI can be found in appendix B.

Use of the the GUI is relatively straight forward, and is broken into three basic steps: preprocessing, processing, and post processing.

The preprocessing step sets up the data into multiple well-defined tasks. The first step is to define what fuels are going to be processed, figure B.1. This is accomplished by entering the fuel names into the list. The next step is to define what data will be analyzed, figure B.2. In this step a Look Up Table(LUT) can be defined to ensure

accurate and quick setting of experimental data, figure B.3. As the folders of the selected data are entered into the list, the environmental conditions may be auto loaded from the LUT. A typical LUT is a comma separated value, or CSV file, as shown in table B.1. Then options are defined for the two processing methods, CVS and TDSA, figure B.4. The last part of the preprocess step is to start generating the associated task files, figure B.5. For the current research, a new task for each movie was generated. This results in 24, 800 tasks (62 experiments $\times$ 100 cycles per experiment $\times$ 4 cameras).

The processing step gives the associated tasks to a distributed computing system, which in turn assigns the tasks to a group of computers. The actual required user work is minimal. A "Start Processing" button, as shown in figure B.6 starts the processing step. A typical run time using 24 computers for 24, 800 tasks requires about 12 hours compute time.

Post processing converts the 24, 800 binary result files in to 4 Excel data workbooks, which equals one workbook for each camera. These workbooks contain a worksheet for each experiment. Every worksheet contains a new column for each cycle in the experiment. The post processing interface is shown in figure B.7.

Chapter 7

Analysis and Discussion

Ten fuels were used to test the capabilities of the apparatus and analysis techniques. These fuels were received from Afton Chemical specifically for this test. The test was setup, such that only random names of the fuels were known, such as "R06000134".

Out of the ten fuels, two fuels were listed as base fuels while the other eight fuels were listed as base fuel plus additive. Figure 7.1 shows how the fuels were grouped together. This information is important so relative comparisons can be made.

7.1 Raw data

Several results need to be discussed, starting with raw data and working toward more complicated analysis. Figures 7.1 and 7.2 show raw data from channel 0 or $3.8\mu m$ wavelength camera. At this wavelength, radiation from the combustion process is at a minimum. The bulk of the radiation seen here is from the cylinder head, which has a high emissivity. In these images, the spark plug (center of image) and the exhaust valves (bottom and right of image) are visible. Figure 7.9 is a view of the cylinder head for comparison.

Both sets of images are similar: fuels A and B show a decrease in cylinder head temperature, while fuels C and D tend to show an increase in cylinder head temperature compared to the base fuel. In figure 7.2 fuel A and B both show a remarked decrease in cylinder head temperature.

Figures 7.3 and 7.4 are the raw data from channel 1 or $2.09\mu m$. This wavelength corresponds to radiation from mostly water. Figures 7.5 and 7.6 are the raw data from channel 2 or $3.48\mu m$. This wavelength is of ethylene, formaldehyde, water, and other unknown species from combustion [12]. Figures 7.7 and 7.8 are from channel 3

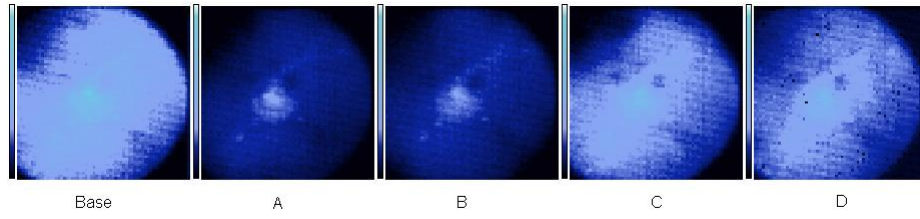| Fuel Name	Base Fuel
GFR-272-A01	R05007191-L01
GFR-272-B01	R05007191-L01
GFR-272-C01	R05007191-L01
GFR-272-D01	R05007191-L01
GFR-273-A02	R06000134
GFR-273-B01	R06000134
GFR-273-C01	R06000134
GFR-273-D01	R06000134

Table 7.1: Fuel Group information
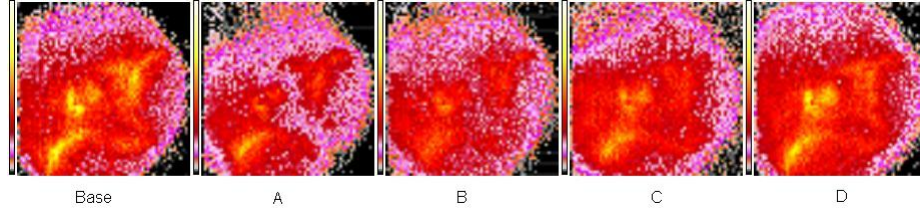
Figure 7.1: Raw Data from Channel 0 at 13° aTDC, from left to right: R05007191-L01, GFR-272-A01, GFR-272-B01, GFR-272-C01, GFR-272-D01
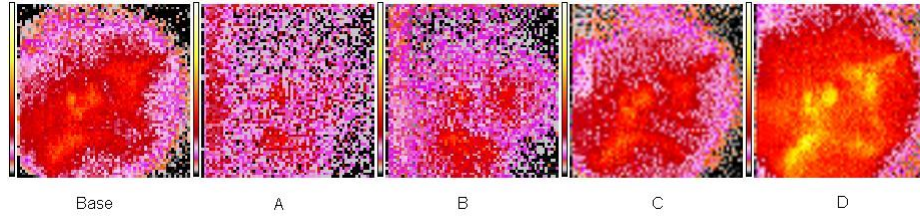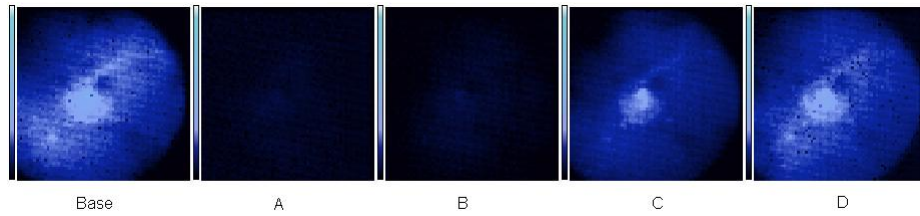

Figure 7.2: Raw Data from Channel 0 at 13° aTDC, from left to right: R06000134, GFR-273-A02, GFR-273-B01, GFR-273-C01, GFR-273-D01
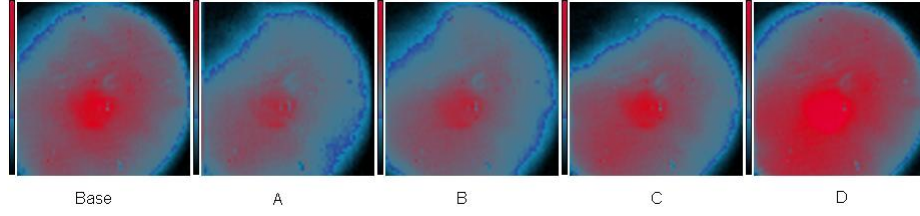
Figure 7.3: Raw Data from Channel 1 at 13° aTDC, from left to right: R05007191-L01, GFR-272-A01, GFR-272-B01, GFR-272-C01, GFR-272-D01
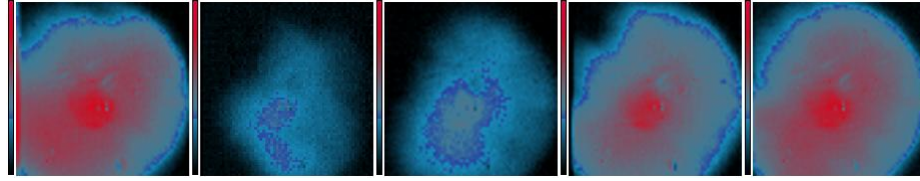
Figure 7.4: Raw Data from Channel 1 at 13° aTDC, from left to right: R06000134, GFR-273-A02, GFR-273-B01, GFR-273-C01, GFR-273-D01
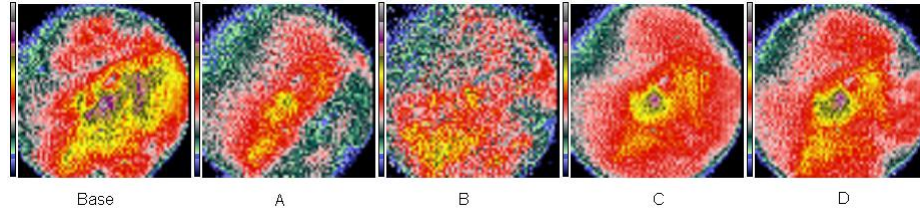
Figure 7.5: Raw Data from Channel 2 at 13° aTDC, from left to right: R05007191-L01, GFR-272-A01, GFR-272-B01, GFR-272-C01, GFR-272-D01
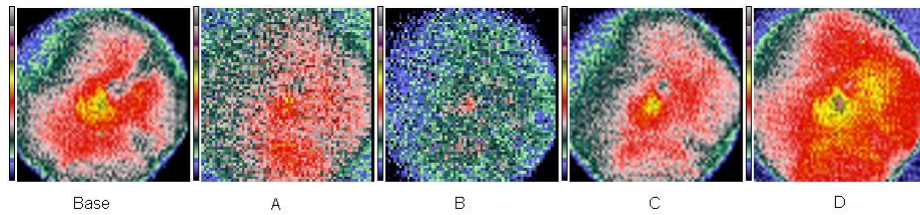
Figure 7.6: Raw Data from Channel 2 at 13° aTDC, from left to right: R06000134, GFR-273-A02, GFR-273-B01, GFR-273-C01, GFR-273-D01

Figure 7.7: Raw Data from Channel 3 at 13° aTDC, from left to right: R05007191-L01, GFR-272-A01, GFR-272-B01, GFR-272-C01, GFR-272-D01

Figure 7.8: Raw Data from Channel 3 at 13° aTDC, from left to right: R06000134, GFR-273-A02, GFR-273-B01, GFR-273-C01, GFR-273-D01

Figure 7.9: View of the valves from the perspective of the camera system.

or $2.47\mu m$, which is also mostly water. Figure 7.2 summarizes the camera information. From these images, it is obvious this trend that fuels A and B seem to be less intense, while fuels C and D seem to be more intense than the base fuel.

Channel	Wavelength	What Generally Seen
0	$3.80\mu m$	Cylinder Head
1	$2.09\mu m$	Water
2	$3.48\mu m$	Ethylene, Formaldehyde, Water, Unknown
3	$2.47\mu m$	Water

Table 7.2: Camera Wavelength information

No information can be definitively extracted directly from these images. Many techniques have been developed to produce some means of interpreting the data, including the band ratio technique[7], adiabatic flame temperature[18], and characteristic vector set[14]. The TDSA method described in depth in chapter 6 will be used here.

7.2 Time Derivative Spatial Averaging analysis

The TDSA method was applied to all of the cameras, however, channel 2 will be analyzed more in depth. This channel was singled out because previous work by Ippolito[11] suggested a wavelength of $3.48\mu m$ is useful for absolute statistical analysis, such as the characteristic vector set method. It will also be shown that channel 2 does offer interesting insight about the fuel additives compared to the base fuels.

A typical result from the TDSA method can be seen in figure D.1. The x-axis is engine crank angle with $0°$ being top dead center of the compression/combustion strokes. The y-axis is the changing rate of intensities of the images. The $\frac{1801.8}{s}$ is the units for the y-axis; this is actually $\frac{1}{5.55\times10^{-4}s}$ which is the frame rate of the cameras. Intensity, in this case, is dimensionless. A region of most interest is between the crank angles $-3° \rightarrow 29°$. This region is of interest since combustion starts at about $-3°$ and is mostly finished by about $30°$ aTDC.

Figures D.1, D.2, D.3, and D.4 are the results from processing the channel 0 images

by the TDSA method. As expected the data is erratic, and nonsensical; as this does not accurately represent the combustion process, but rather it is similar to the cylinder head temperature. It was processed to verify that the initial thoughts about channel 0 were correct.

Figures D.5, D.6, D.7, and D.8 are the results from processing channel 1. Being that this channel represents mostly water during the combustion process, it is not surprising that all of the curves are very similar; except for fuel GFR-273-B01 which suggests the data for that fuel may be suspect.

Figures D.13, D.14, D.15, and D.16 show the results from channel 3. Being that channel 1 and 3 are both of mostly water, they should be similar. When comparing figure D.5 to figure D.13 the curve similarities are apparent. It is easiest to compare a ratio of ratios, to put this in mathematical form, equation 7.1. The average of the ratios, across the region of interest approximately a crank angle of $-3°$ to $29°$, is then calculated. This "region of interest" is the crank angle range when combustion occurs. This ratio for GFR-272-A01, GFR-272-B01, GFR-273-A02, GFR-273-B01 is less than 5% for all. This indicates that variations seen between channel 1 and channel 3 may be attributed to the emissive differences of water between the two wavelengths.

$$mean \left\{ \frac{\frac{dF}{dt}\big|_{channel1, GFR-272-A01}}{\frac{dF}{dt}\big|_{channel1, R05007191-L01}} \cdot \left[\frac{\frac{dF}{dt}\big|_{channel3, GFR-272-A01}}{\frac{dF}{dt}\big|_{channel3, R05007191-L01}} \right]^{-1} \right\}_{crankangle -3 \rightarrow 29} \tag{7.1}$$

This ratio of ratios does not work for the other four fuels (GFR-272-C01, GFR-272-D01, GFR-273-C01, GFR-273-D01); the emission spectrum near $2.47\mu m$ does not seem to be affected by the fuel additives. The curves for all four fuels are nearly identical and follows that of the appropriate base fuel.

The last channel, channel 2, should be considered most important because the wavelength is within the range of the emission spectrum of ethylene and formaldehyde; both of these species are important in the burning of hydrocarbons. Most notably of all, both species are not prevalent in the final combustion products (assuming complete combustion). This then has the ability to follow the combustion phenomena as it occurs rather

than seeing the result of combustion.

During the original analysis, this method predicted the fuels GFR-272-A01, GFR-272-B01, GFR-273-A02, and GFR-273-B01 had an octane improver added. Also, it was predicted that fuels GFR-272-C01, GFR-272-D01, GFR-273-C01, and GFR-273-D01 had a cetane improver added. While the analysis did not have the luxury of having the fuel data and the fuel additive information, it would seem sensible to explain the fuels now. This will let phenomena determined by the TDSA method be explained by known fuel information.

Property	R05007191L01	R06000134
Specific Gravity	0.7424	0.7463
Aromatics Volume	26.3%	34.3%
Olefins Volume	13.8%	9.1%
Oxygen Content	0%	0%
Sulfur Weight	0.0156%	0.00084%
Research Octane	91.2	95.6
Motor Octane	82.2	85.1
Anti-Knock Index	86.7	90.4
Carbon Content	85.74%	87.53%
Hydrogen Content	14.17%	12.47%
BTU/lb	19222	19609

Table 7.3: Base fuel information

Table 7.3 shows properties of the two base fuels. The only properties of interest to this research are the octane ratings and the anti-knock index(which is the average of the octane ratings). Table 7.4 shows the eight fuels with the associated base fuels, the fuel additives, and the amount of additive per 4 gallons of base fuel. From this, it could be assumed that fuel GFR-272-B01 should react in a similar, but more significant way than GFR-272-A01.

Figure 7.10 shows the results of the TDSA analysis on 3 fuels: R05007191-L01, GFR-272-A01, and GFR-272-B01. Figure 7.11 shows similar results on 3 fuels: R06000134,

Fuel Name	Base Fuel	Additive	Additive(g) per 4 Gallons Base Fuel
GFR-272-A01	R05007191-L01	N-Methylaniline	30.4g
GFR-272-B01	R05007191-L01	N-Methylaniline	76g
GFR-272-C01	R05007191-L01	Diphenylamine	48g
GFR-272-D01	R05007191-L01	Diphenylamine	120g
GFR-273-A02	R06000134	N-Methylaniline	30.4g
GFR-273-B01	R06000134	N-Methylaniline	76g
GFR-273-C01	R06000134	Diphenylamine	48g
GFR-273-D01	R06000134	Diphenylamine	120g

Table 7.4: Fuel additive information

GFR-273-A02, and GFR-273-B01. Since these four (non-base) fuels are similar in that they all have N-Methylaniline added, they will be analyzed together. First, note that N-Methylaniline is an octane improver, which means that as a fuel burns, it should be a less reactive mixture overall.

Start with fuel GFR-272-A01, in figure 7.10, and notice the significant drop in amplitude, with respect to the base fuel, from the effects of the fuel additive. The lower amplitude indicates less overall reactivity. Fuel GFR-273-A02, in figure 7.11, does have a drop, however, the drop is not as substantial as in GFR-272-A01. This can be readily explained by the octane ratings of the base fuels; R05007191-L01 has a lower octane rating, and, thus, is more susceptible to the effects of the octane improver.

Moving to fuel GFR-272-B01, it is clear that by adding more N-Methylaniline it decreased the amplitude more; which means the reactivity of the overall mixture has fallen. However, the decrease in reactivity is not linearly related to the amount of additive. While R050007191-L01 is more susceptible to the effects of the additive, it is also more susceptible to becoming chemically immune to the effects; i.e. adding more additive will eventually have no effect on octane rating.

The data associated with fuel GFR-273-B01 may be meaningless, as previously noted. However, it could also mean that having a relatively high octane rating, and

adding a large amount of octane improver, may have a devastating impact on the combustion process. Unfortunately, from the current research, it is not possible to tell which is the case.

Figure 7.12 shows the results for 3 fuels: R05007191-L01, GFR-272-C01, and GFR-272-D01. Similarly figure 7.13, is the results for: R06000134, GFR-273-C01, and GFR-273-D01. These four (non-base) fuels all have diphenylamine added. Diphenylamine is not a cetane improver as predicted, however, it is a combustion improver. A combustion improver tends to smooth the combustion process while making the combustion more complete; it also has the effect of decreasing ignition delay. Cetane improvers tend to decrease ignition delay.

GFR-272-C01 does not show a decrease in ignition delay (rising curve shifted to left) compared to the base fuel; this may be explained by the octane rating of the fuel; it is relatively low and thus may not be able to reduce the ignition delay further. The amplitude is higher as the "more complete combustion" would suggest.

GFR-273-C01 has a curve rising earlier than that of the base fuel. However, the amplitude did not increase, which can be explained again by the base fuel's octane rating. The higher octane rating is less susceptible to the smoothing and more complete combustion effects of the combustion improver; while being more susceptible to the reduction in ignition delay effect.

GFR-272-D01 shows only a marginal increase in amplitude over GFR-272-C01. The effects of smoothing the combustion process is readily seen by forcing the combustion process to burn longer than that of GFR-272-C01 (an extension of the peak to the right). As with the n-methylaniline, R05007191-L01 tends to become chemically immune to the effects of the fuel additive.

GFR-273-D01 has a significant increase in amplitude and a marginal increase in combustion smoothing effects. The ignition delay was shortened slightly. These effects can again be attributed to chemical processes, and how susceptible a fuel is to change based upon its chemical makeup.

These chemical effects were verified by the chemical corporation which supplied the fuels, Afton Chemical; including the susceptibility of each fuel to the respective

additives.

It may seem reasonable to compare R05007191-L01 to R06000134, however, this is not practical. Gasolines have many constituents. These various species may burn, to produce more or less of the important ethylene and formaldehyde species; which is visible by means of this particular wavelength camera. Also, the total amount of energy the gasoline contains can significantly alter the temperature within the combustion chamber; which would alter how the fuel burns. Therefore, this method should be restricted to a base fuel and a fuel additive for use as a comparison, and not two completely differing fuels.

Unfortunately, error analysis based upon this method is, at this time, impossible. The inherent cyclic variability of the internal combustion engine, makes all standard error analysis meaningless; since cycle-to-cycle variations may be as large as 100%. This is the largest reason why the analysis is purely qualitative and not a quantitative analysis.

The results and accuracy of the flame propagation tracking and characteristic vector sets method were not included, since the ultimate goal of this research was to develop a tool based upon the TDSA method.
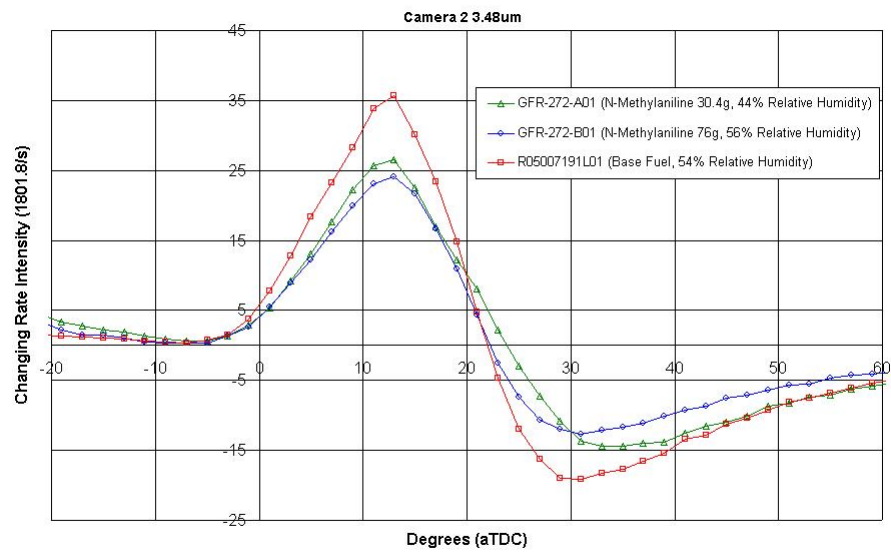
Figure 7.10: TDSA results for R05007191-L01, GFR-272-A01, and GFR-272-B01 for channel 2 (3.48μm)

Figure 7.11: TDSA results for R06000134, GFR-273-A02, and GFR-273-B01 for channel 2 (3.48μm)
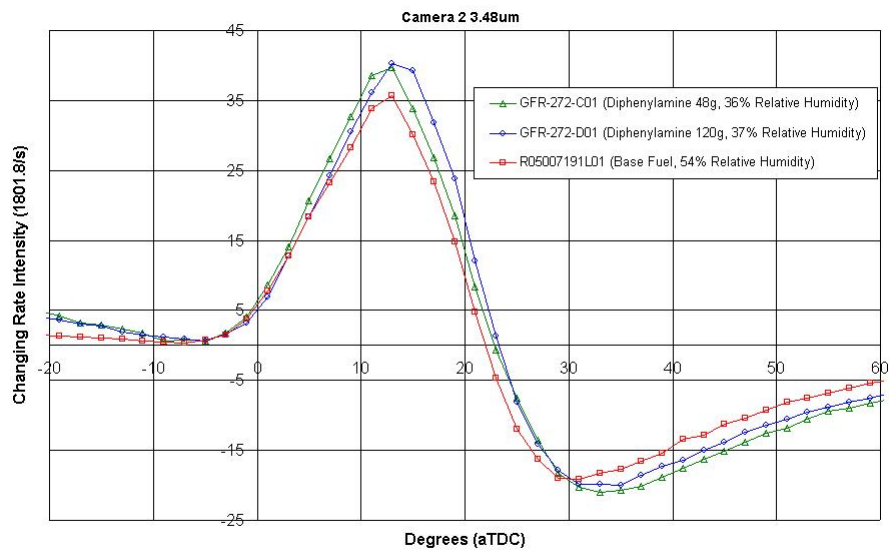
Figure 7.12: TDSA results for R05007191-L01, GFR-272-C01, and GFR-272-D01 for channel 2 (3.48μm)
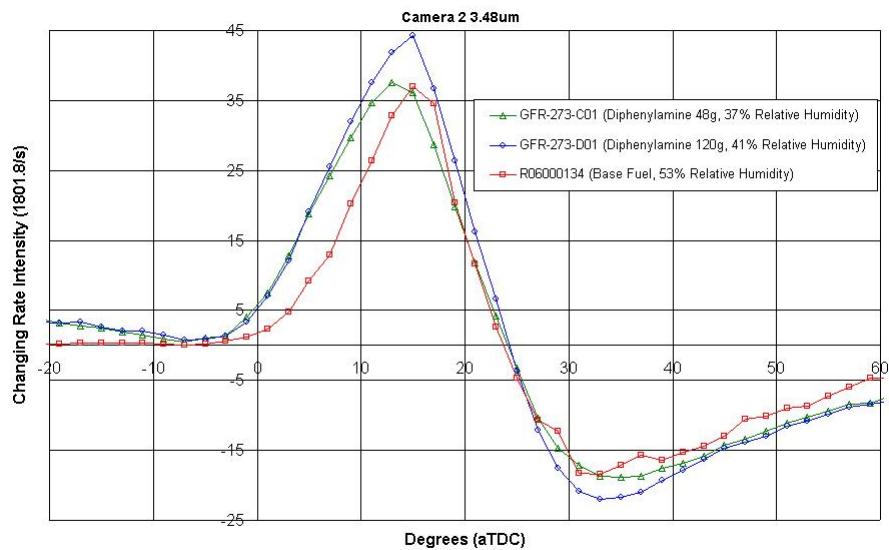
Figure 7.13: TDSA results for R06000134, GFR-273-C01, and GFR-273-D01 for channel 2 (3.48μm)

Chapter 8

Conclusion

In-cylinder combustion processes were studied by means of a high speed multi-spectral infrared camera system, called the Rutgers Super Imaging System (SIS). The images were analyzed by a novel robust statistical analysis method. Experimental variables included fuel and fuel additives.

The imaging system is capable of recording four spatial images simultaneously at wavelengths of $3.8\mu m$, $2.09\mu m$, $3.48\mu m$, $2.47\mu m$. The Super Imaging System is aligned with a Bowditch style optical access engine. This engine required modifications to achieve better results. It is close to a real world engine, for example, it uses metallic rings and oil on the optical piston.

The statistical analysis tool has many tools integrated into it. These include the characteristic vector set method, flame front tracking, time derivative spatial averaging (TDSA), and robust statistics tools. TDSA uses a time derivative to reduce the pixel errors, which may occur. Using this method, the wavelength of $3.48\mu m$ seemed to have the most successful means of predicting fuel additive effects. This is reasonable since ethylene and formaldehyde both have spectral bands covering $3.48\mu m$.

The predictions from the TDSA method were accurate for four of the fuels; the method predicted an octane improver was added to the base. The other four were conceptual correct; the method predicted cetane improver was added, however, a combustion enhancer was added. Cetane improvers and combustion enhancers have similar effects on fuels. The actual fuel and fuel additive properties were reported by the fuel supplier, Afton Chemical.

8.1   Future Work

Many steps should be considered after this work. The cyclic variations from the engine need to be eliminated from the calculations; using standard error analysis the error calculations currently result in standard deviations of about 40%.

A new application, which can accurately define changes between the resultant curves from the TDSA method, needs to be developed. A computer interpretation of the result curves would also eliminate any bias, which may be present. This application would be technically easy to develop, but would require a lot of time; since a large database of curve changes due to specific additives would need to be compiled.

Appendix A

Images of the Redesigned Extended Piston (REP)

Figure A.1: Redesigned Extended Piston after some use
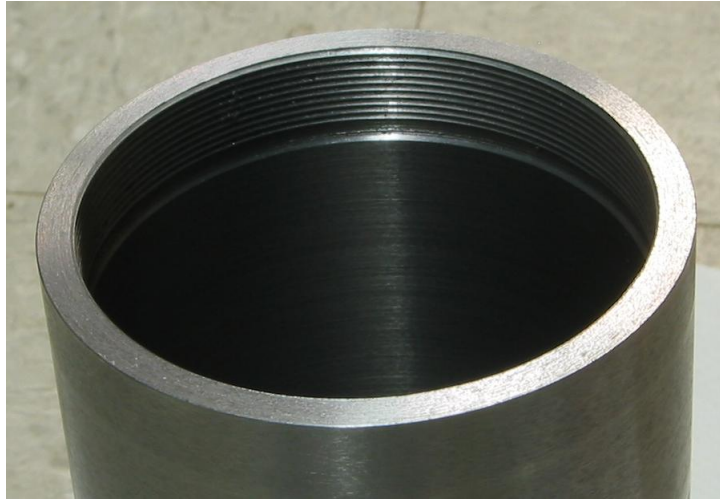
Figure A.2: Close up of the piston bottom
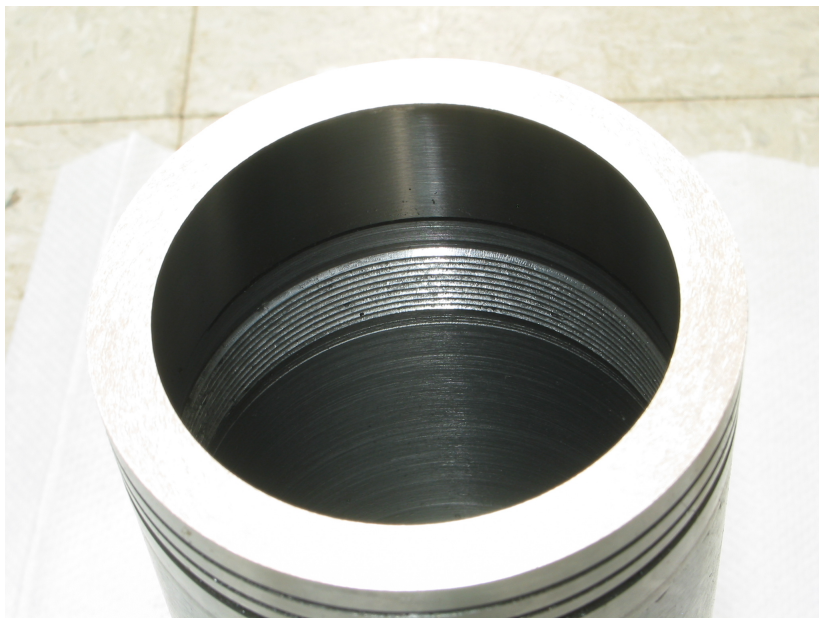
Figure A.3: Close up of the piston top

Figure A.4: REP and its constituents

Figure A.5: Spanner Wrench for threaded lock ring
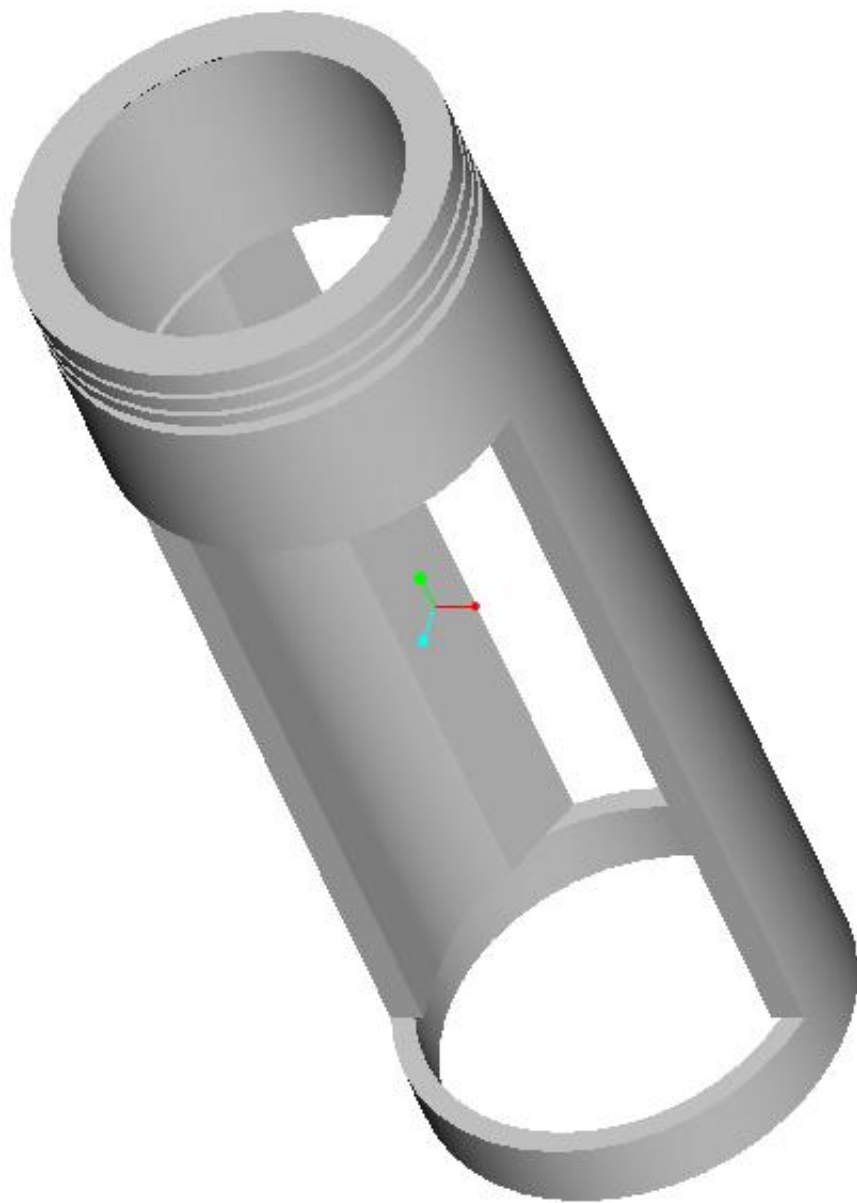
Figure A.6: Isometric view of the REP
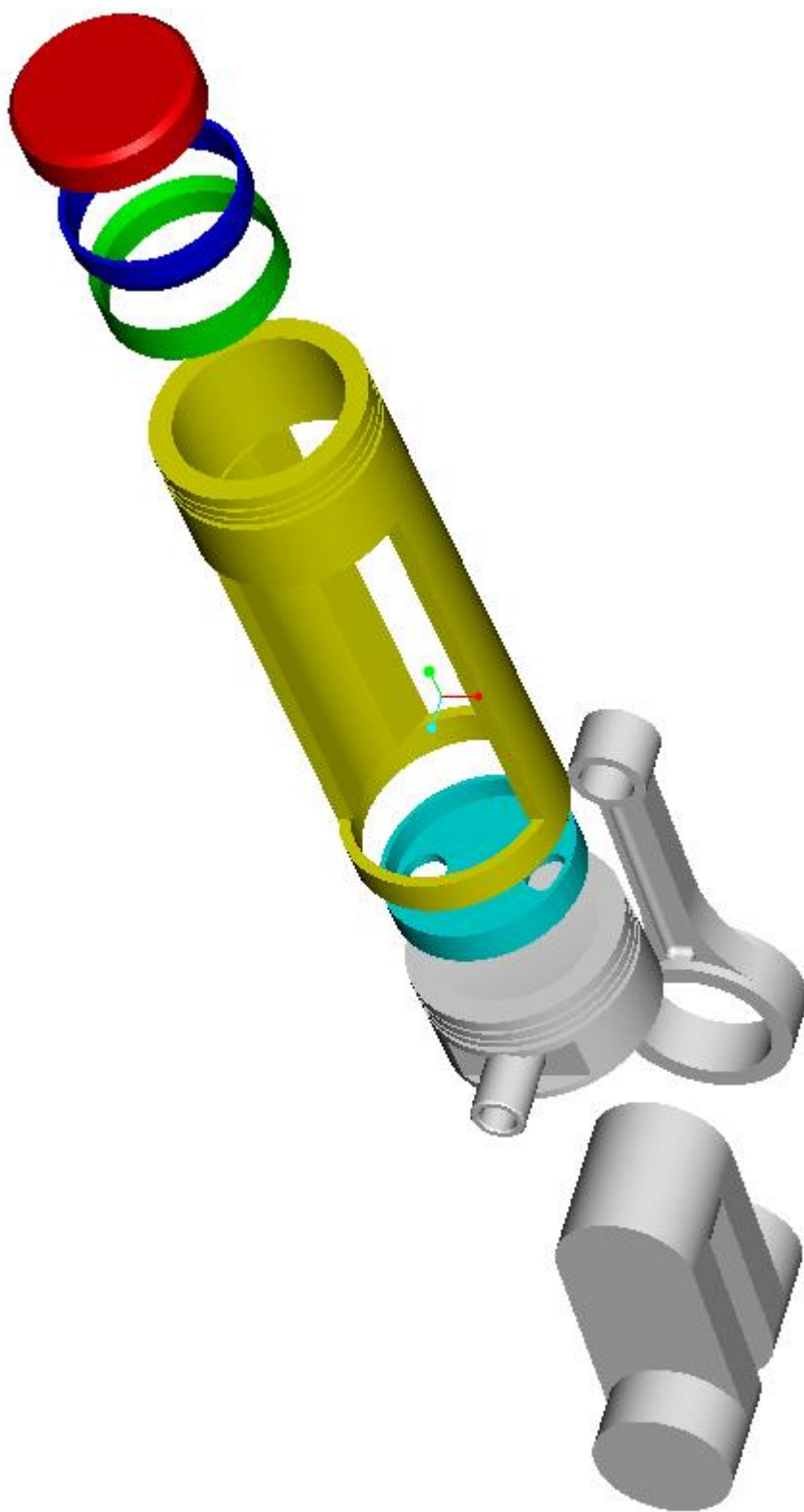
Figure A.7: Exploded view of the optical access piston assembly
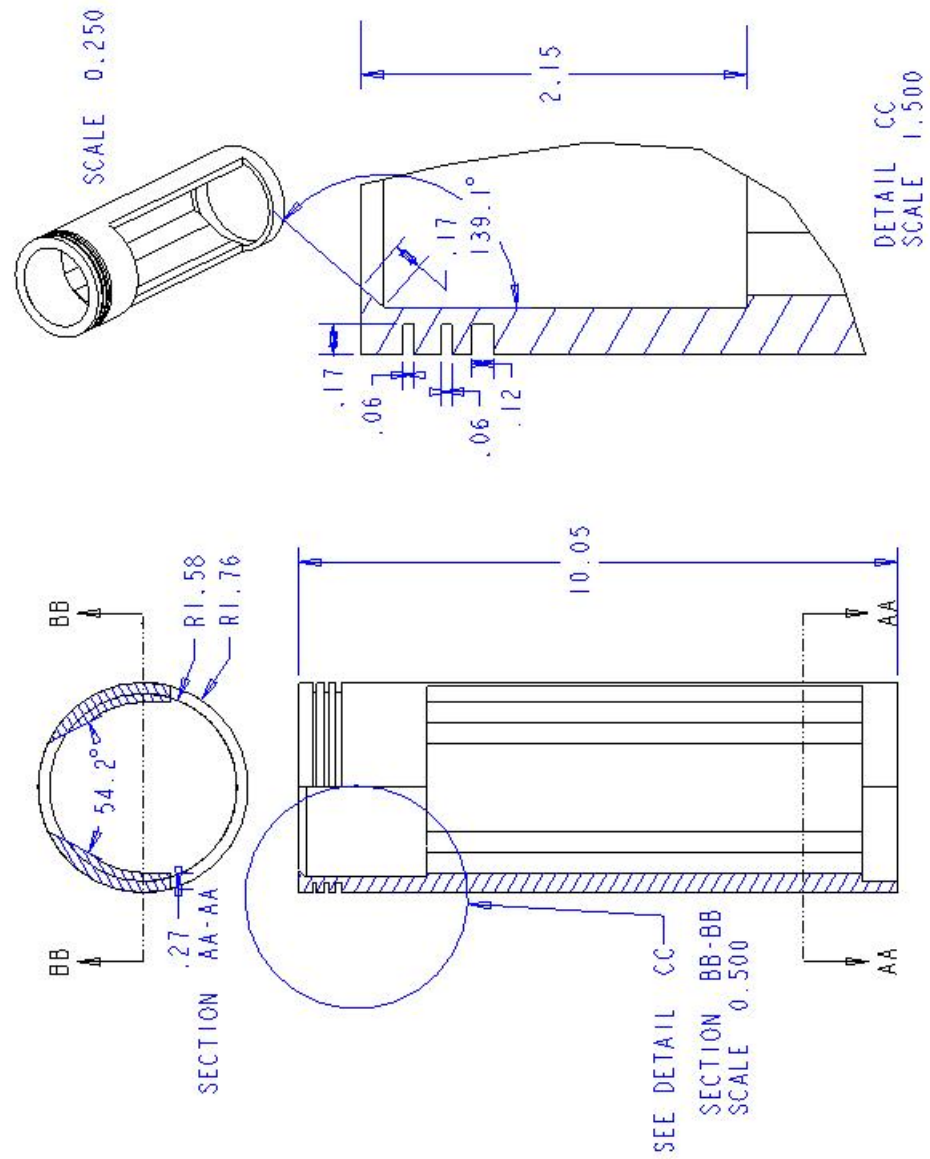
Figure A.8: Mechanical Drawing of REP (Not drawn to scale)

Appendix B

Images of the Rutgers Imaging Application
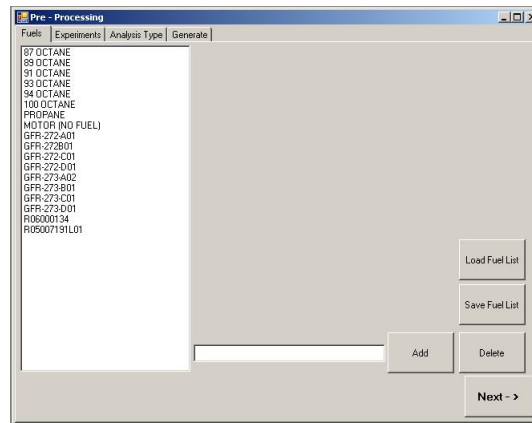
Figure B.1: Preprocess Fuel Panel
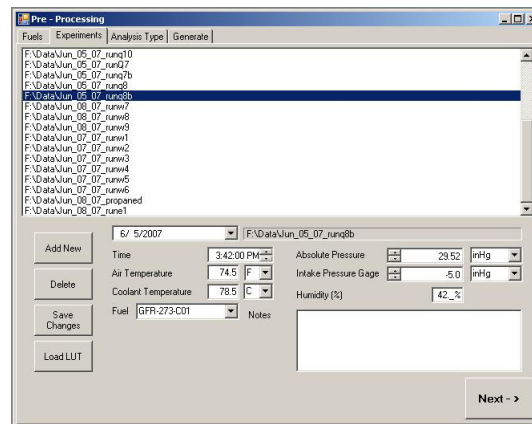
Figure B.2: Preprocess Experiment Panel
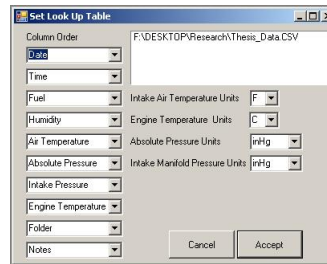
Figure B.3: Preprocess Look Up Table

5/31/2007	2:41 PM	R06000134	44	74.5	30.075	-5	76.1	Run1
5/31/2007	3:31 PM	R05007191L01	46	75.7	30.075	-5	77.5	Run2
5/31/2007	4:24 PM	GFR-272-A01	44	75.7	30.075	-5	77.5	Run3
5/31/2007	5:08 PM	GFR-272-B01	43	75.6	30.075	-5	77.2	Run4
5/31/2007	6:41 PM	GFR-272-D01	44	75.9	30.03	-5	79.1	Run6
5/31/2007	5:33 PM	GFR-272-C01	44	77.1	30.075	-5	78.5	Run5
6/1/2007	12:33 PM	GFR-273-A02	61	76.6	30.04	-5	77.7	Run7
6/1/2007	1:27 PM	GFR-273-B01	58	77	30.04	-5	78.2	Run8

Table B.1: Example LUT; Columns from left to right: Date, Time, Fuel Name, Relative Humdity, Atmospheric Temperature (F), Atmospheric Pressure (in.Hg), Intake Pressure (psig), Engine Coolant Temperature (C), Experiment Folder
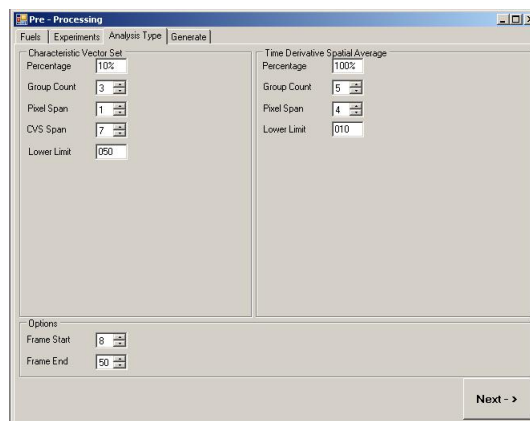
Figure B.4: Preprocess Options Panel
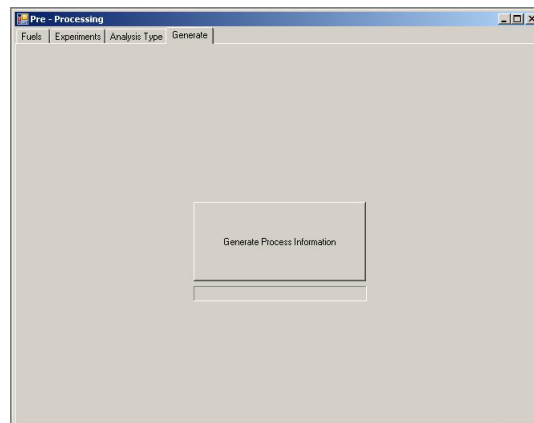
Figure B.5: Preprocess Generate Panel

Figure B.6: Processing Window
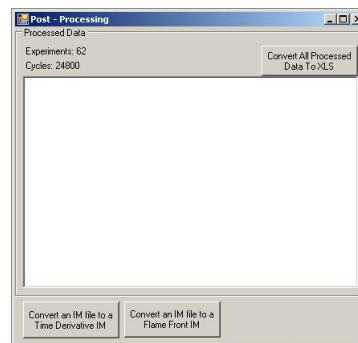
Figure B.7: Post Process Window

Appendix C

Images of Digital Timing Circuit Board
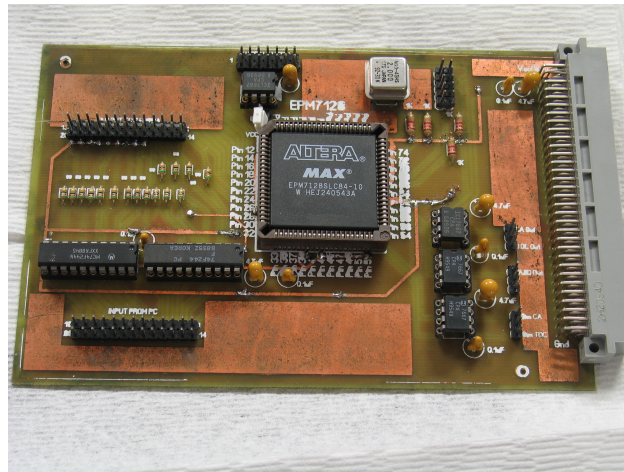
Figure C.1: Front of finished circuit board
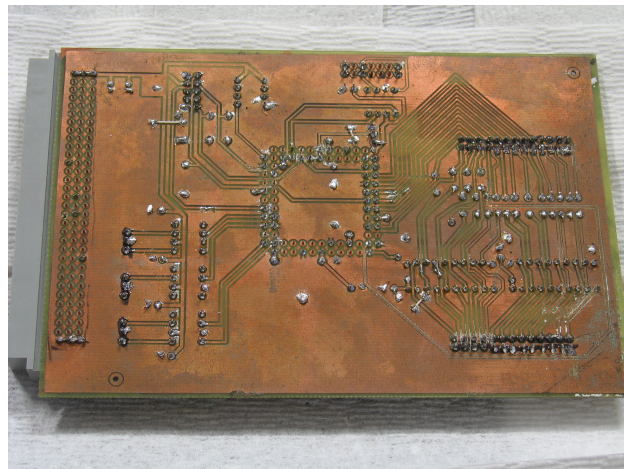
Figure C.2: Back of finished circuit board
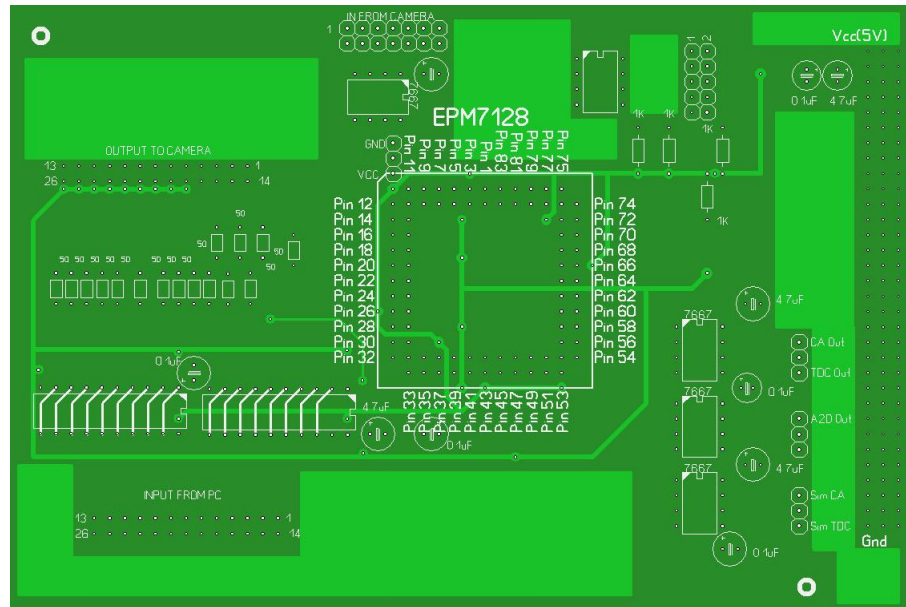
Figure C.3: Front etch mask, with screen print, false colored
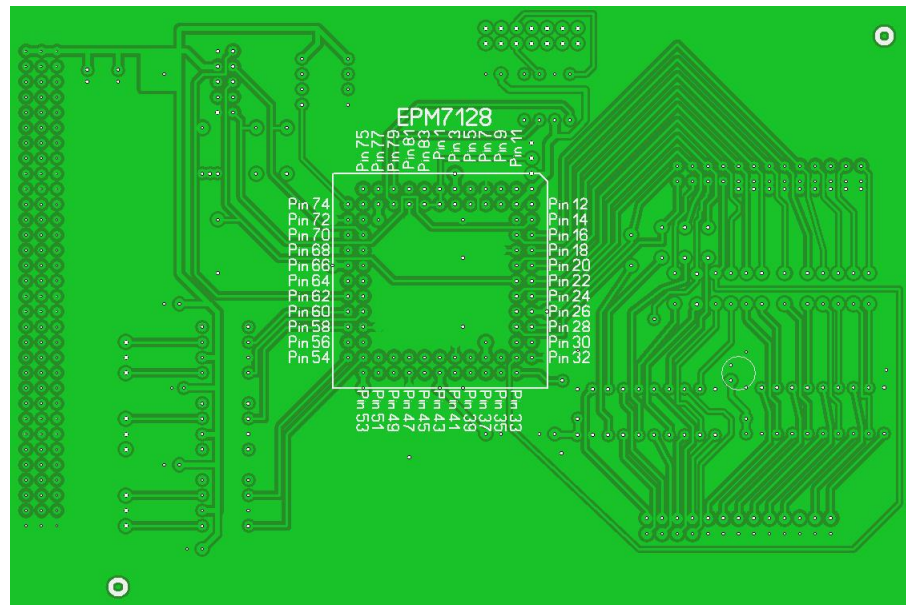
Figure C.4: Back etch mask, with screen print, false colored

C.1 CPLD Program

Program is listed in alphabetical order (except for the main program).
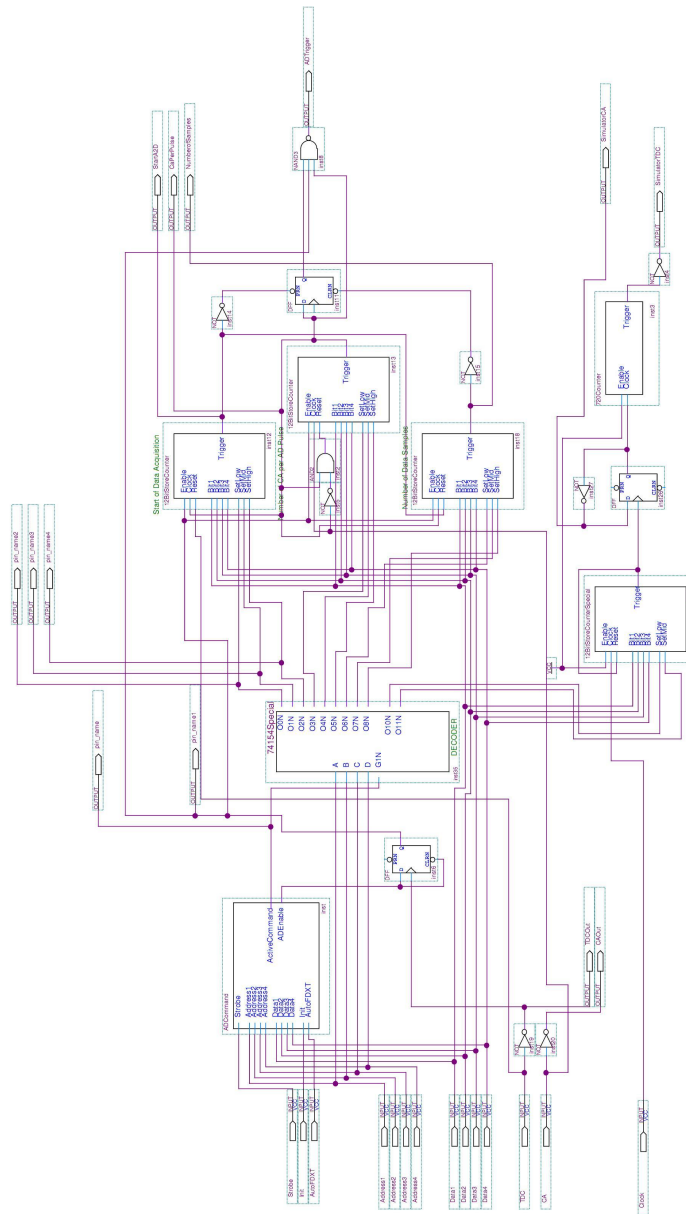
Figure C.5: CPLD Main Program
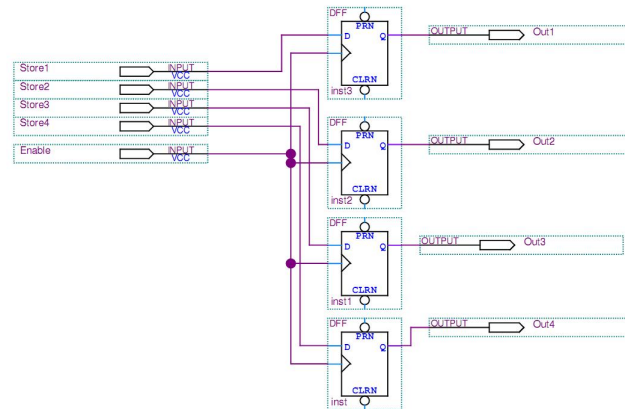
Figure C.6: 4BitLatch
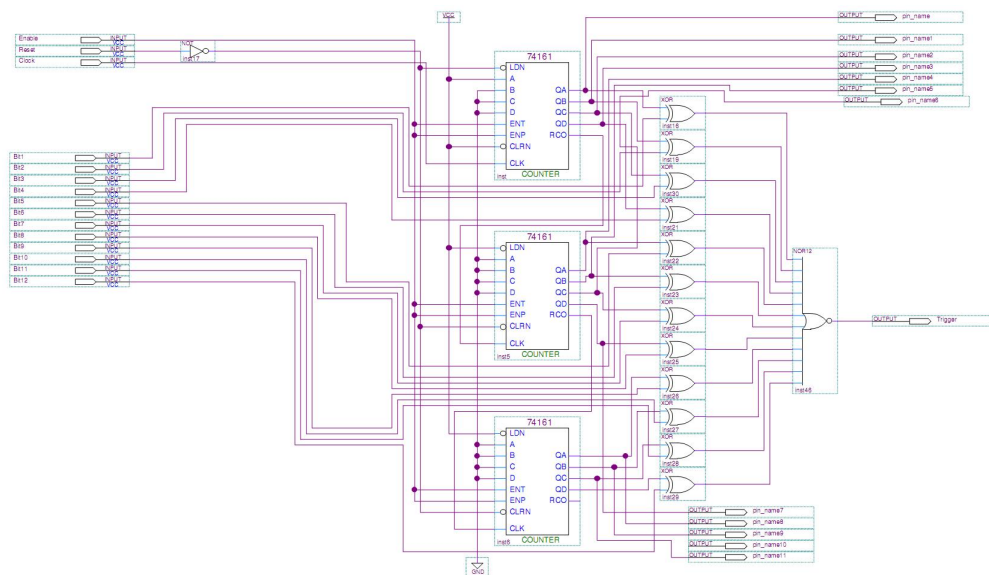
Figure C.7: 12BitCount
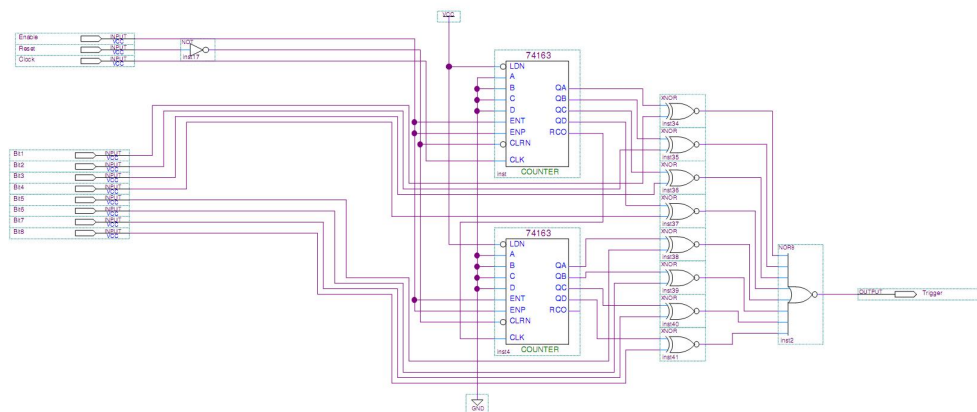
Figure C.8: 12BitCountSpecial
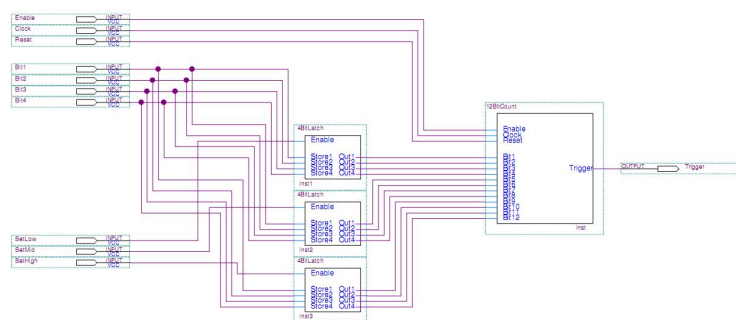
Figure C.9: 12BitStoreCounter
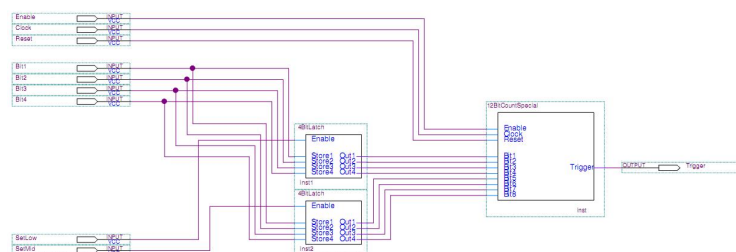
Figure C.10: 12BitStoreCounterSpecial
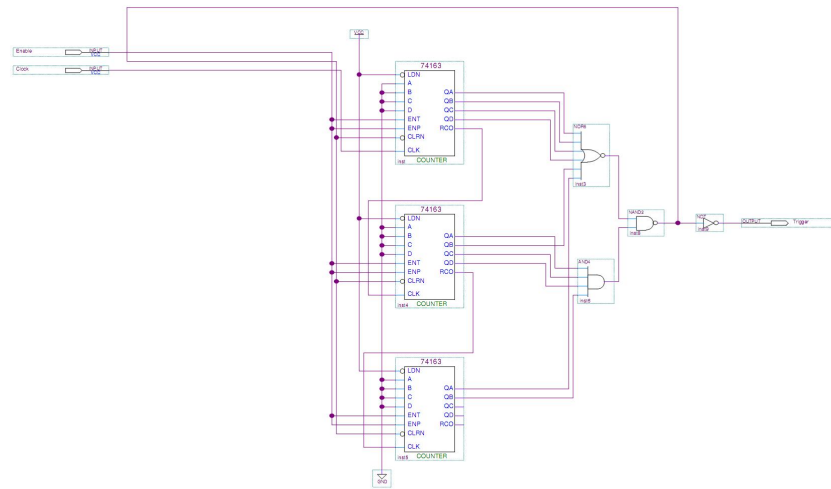
Figure C.11: 720Counter
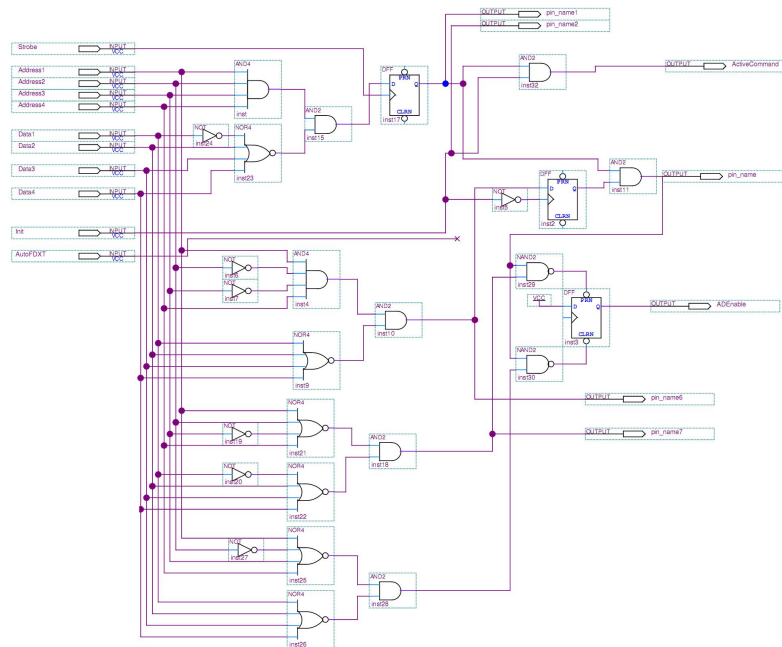
Figure C.12: ADCommand

Appendix D

Analysis Figures
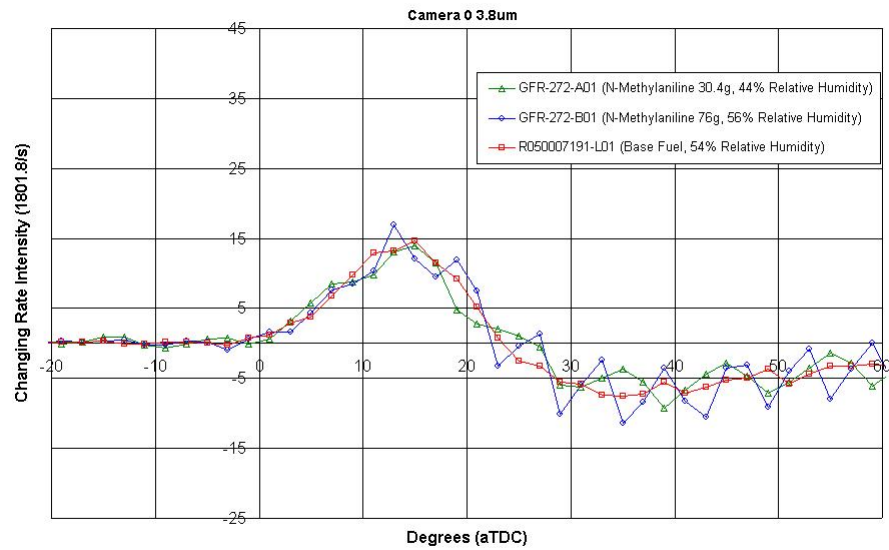
Figure D.1: TDSA results for R05007191-L01, GFR-272-A01, and GFR-272-B01 for channel 0 ($3.8\mu m$)
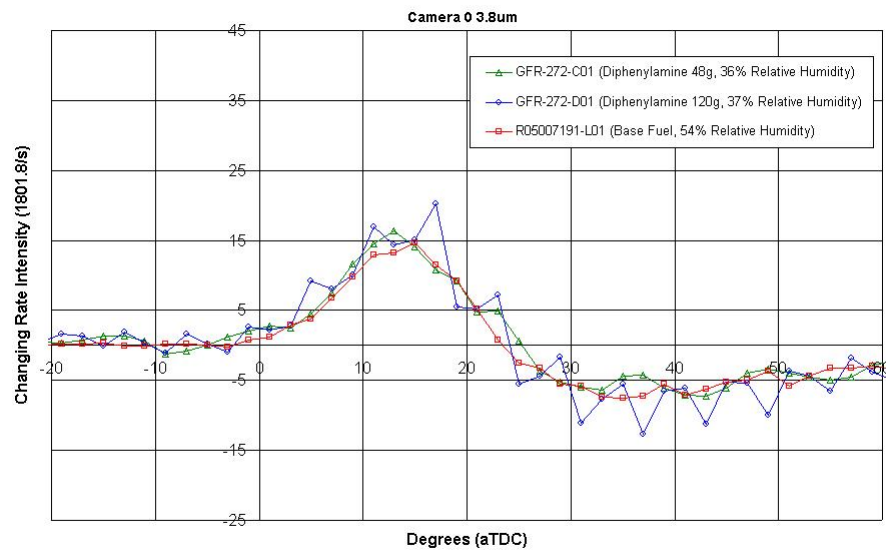
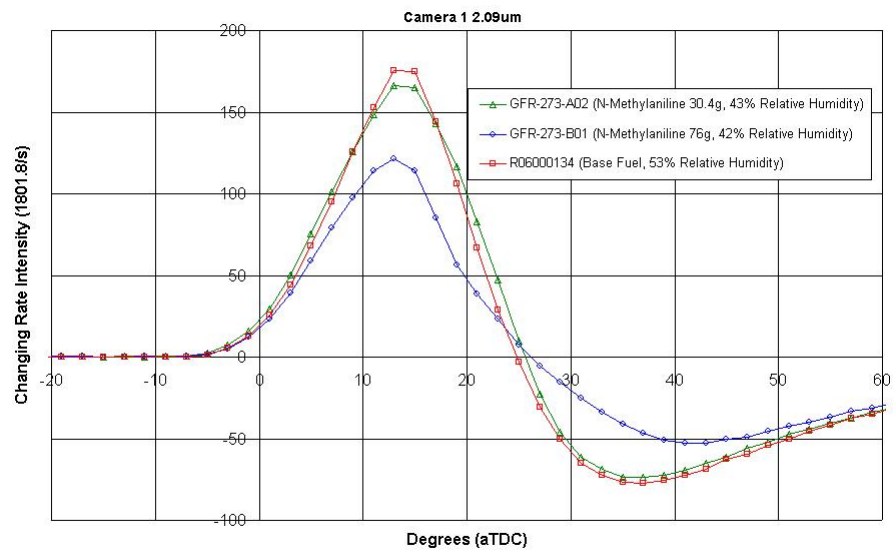Figure D.2: TDSA results for R05007191-L01, GFR-272-C01, and GFR-272-D01 for channel 0 ($3.8\mu m$)
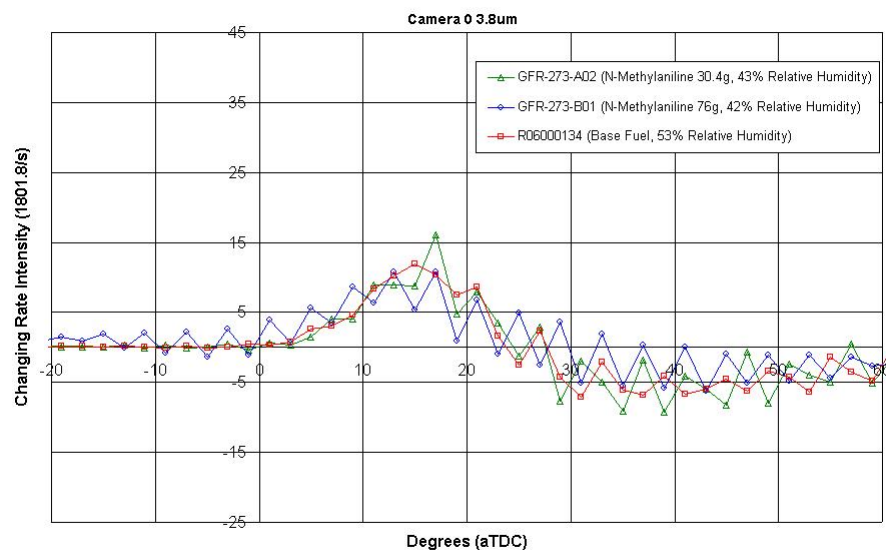
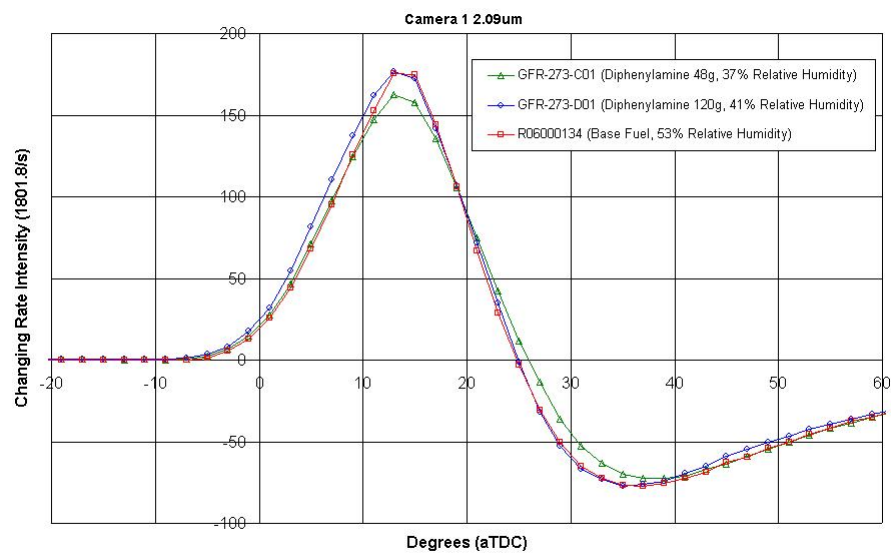Figure D.3: TDSA results for R06000134, GFR-273-A02, and GFR-273-B01 for channel 0 ($3.8\mu m$)
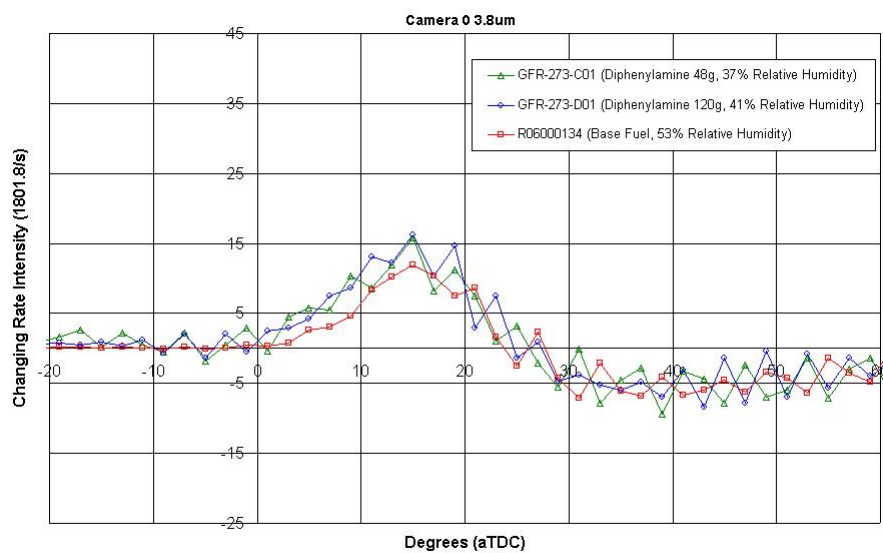
Figure D.4: TDSA results for R06000134, GFR-273-C01, and GFR-273-D01 for channel 0 (3.8μm)
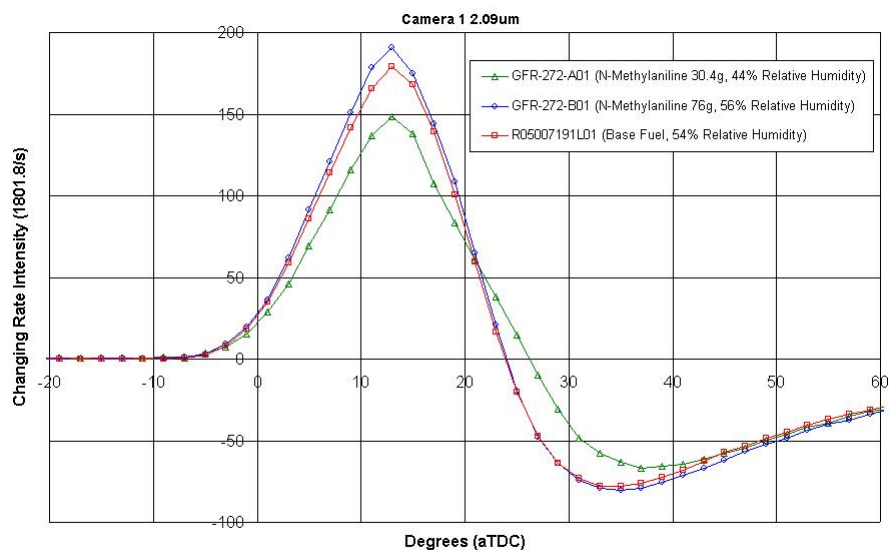
Figure D.5: TDSA results for R05007191-L01, GFR-272-A01, and GFR-272-B01 for channel 1 (2.09μm)
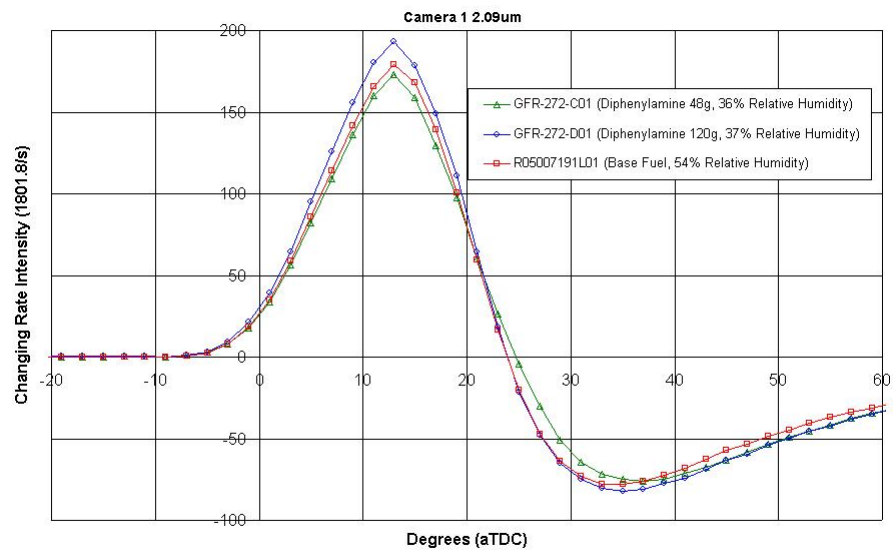
Figure D.6: TDSA results for R05007191-L01, GFR-272-C01, and GFR-272-D01 for channel 1 (2.09μm)

Figure D.7: TDSA results for R06000134, GFR-273-A02, and GFR-273-B01 for channel 1 (2.09μm)

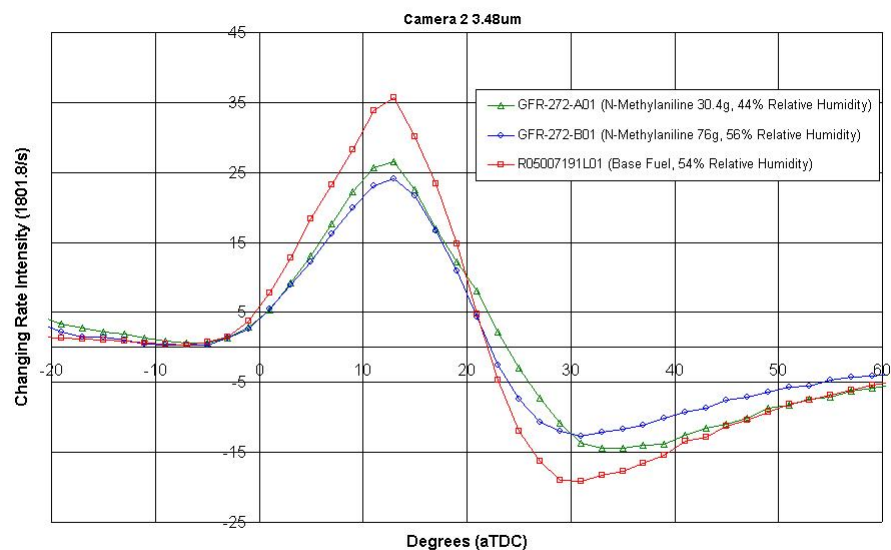Figure D.8: TDSA results for R06000134, GFR-273-C01, and GFR-273-D01 for channel 1 (2.09μm)

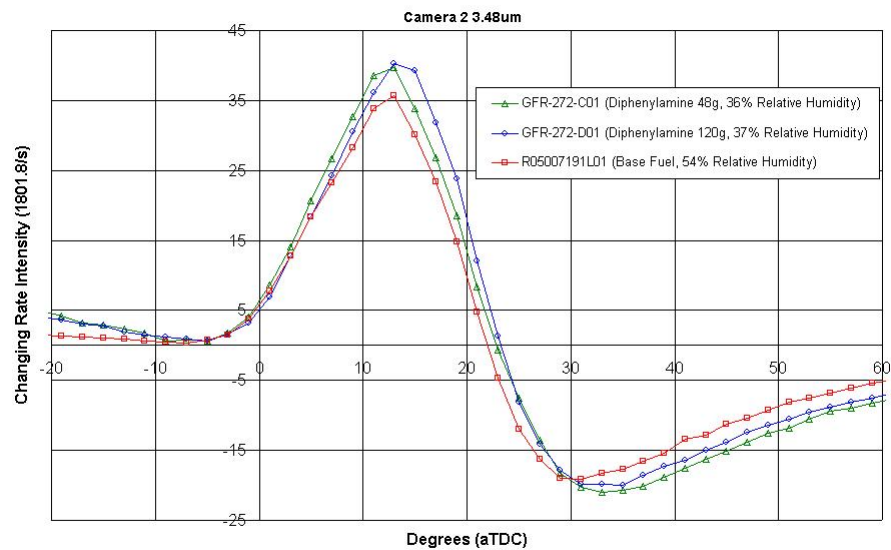Figure D.9: TDSA results for R05007191-L01, GFR-272-A01, and GFR-272-B01 for channel 2 (3.48μm)

Figure D.10: TDSA results for R05007191-L01, GFR-272-C01, and GFR-272-D01 for channel 2 (3.48μm)
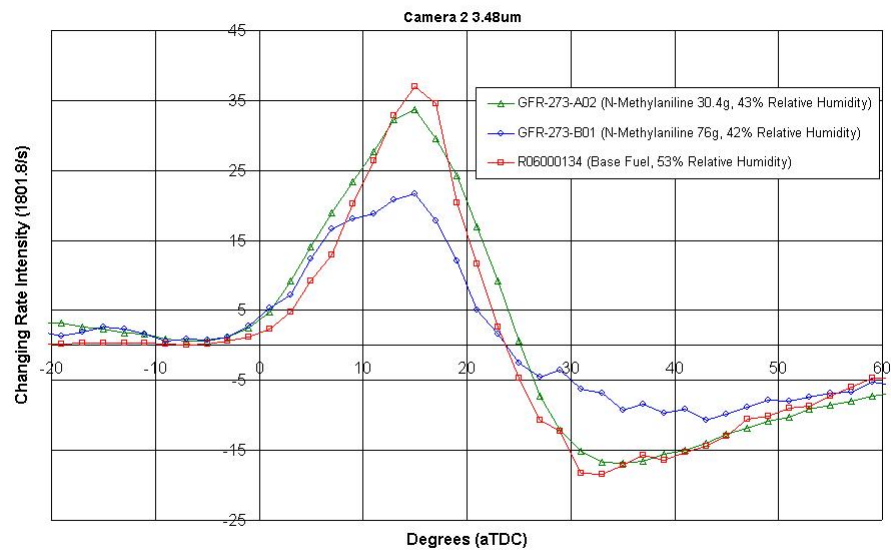

Figure D.11: TDSA results for R06000134, GFR-273-A02, and GFR-273-B01 for channel 2 (3.48μm)
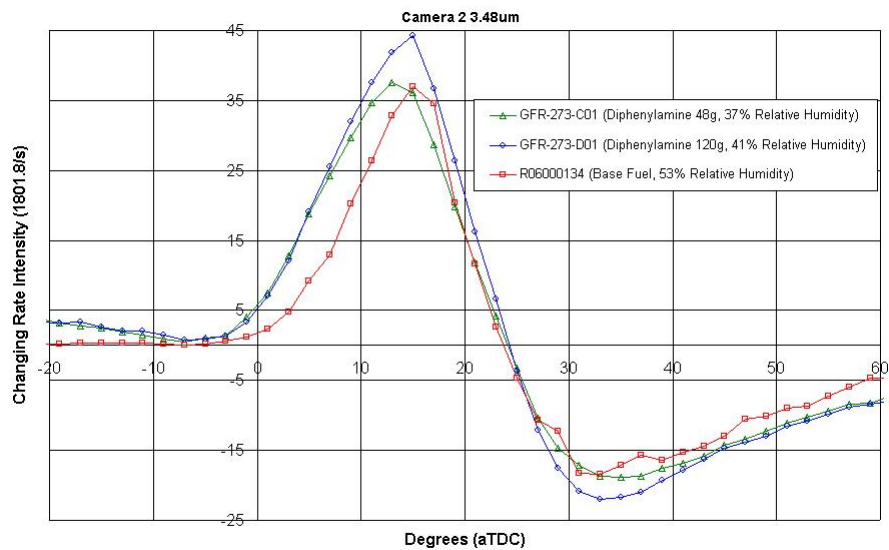
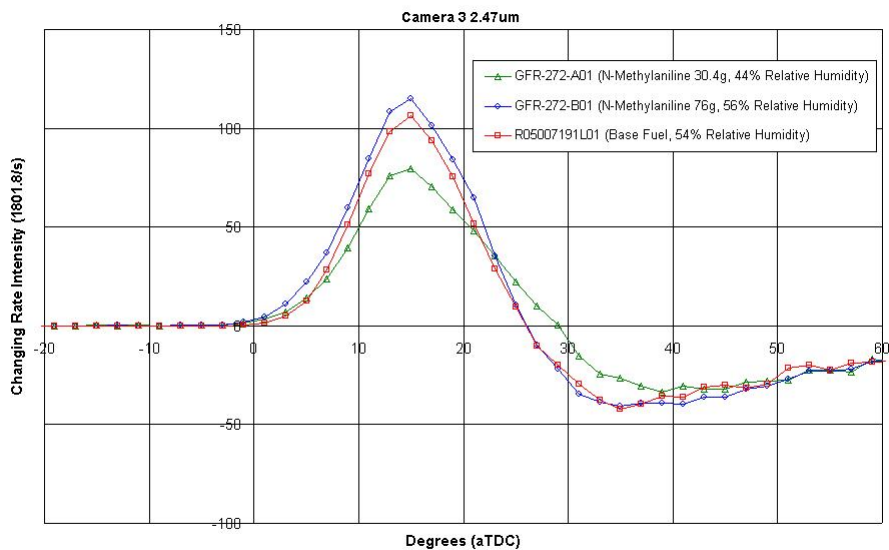Figure D.12: TDSA results for R06000134, GFR-273-C01, and GFR-273-D01 for channel 2 (3.48μm)

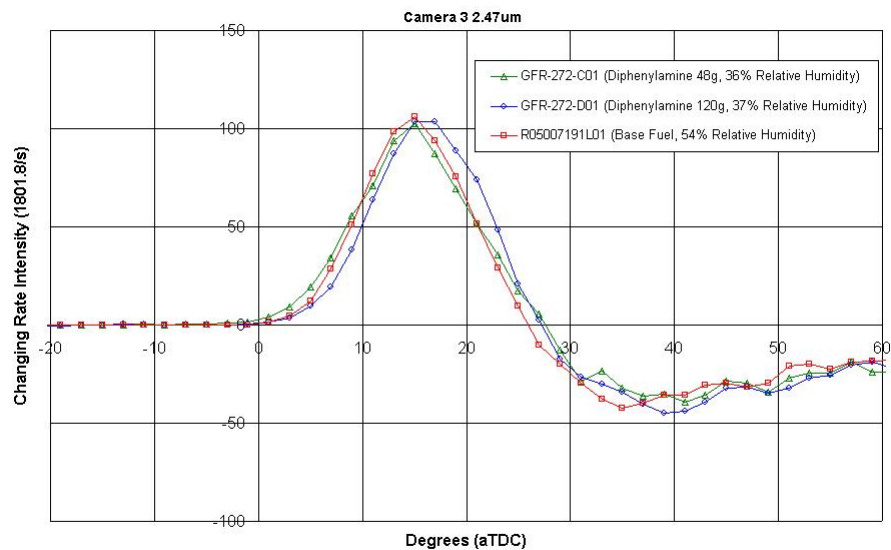Figure D.13: TDSA results for R05007191-L01, GFR-272-A01, and GFR-272-B01 for channel 3 (2.47μm)

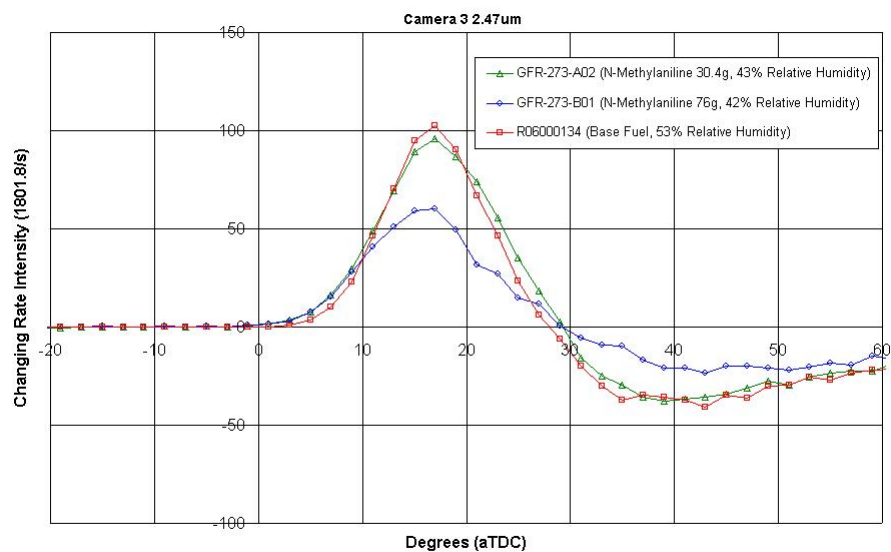Figure D.14: TDSA results for R05007191-L01, GFR-272-C01, and GFR-272-D01 for channel 3 (2.47μm)

Figure D.15: TDSA results for R06000134, GFR-273-A02, and GFR-273-B01 for channel 3 (2.47μm)
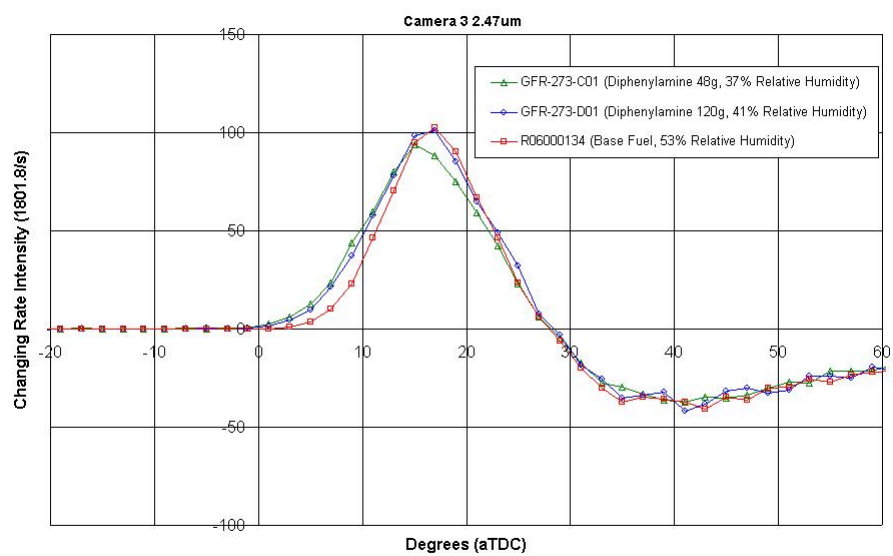
Figure D.16: TDSA results for R06000134, GFR-273-C01, and GFR-273-D01 for channel 3 (2.47μm)

References

[1] 10 by 10 act, amendment to the clean air act. Retrieved January 26, 2006, from http://www.gil.house.gov/IssueItems/10by10/10by10bill.pdf.

[2] Online military publications and engineering documents. http://www.tpub.com.

[3] BACHMAN, J. Blue ribbon panel for reviewing use of mtbe. http://www.epa.gov /OMS/consumer/fuels/oxypanel/blueribb.htm.

[4] CHANG, C., CLASEN, E., SONG, K., CAMPBELL, S., AND RHEE, K. Quantitative imaging of in-cylinder processes by multi-spectral methods. Tech. Rep. SAE Paper 970872, Society of Automotive Engineers, 1997.

[5] COOPER, J. B., WISE, K. L., GROVES, J., AND WELCH, W. T. Determination of octane numbers and reid vapor pressure of commercial petroleum fuels using ft-raman spectroscopy and partial least-squares regression analysis. *Analytical Chemistry vol 67*, no 22 (1995).

[6] FANG, T. Assessment of multi-band spectrometry applied to determination of temperature and species concentration in non-uniform combustion gaseous mixture. Master's thesis, Rutgers University, 2001.

[7] FERRISO, C., LUDWIG, C., AND BOYNTON, F. A band-ratio technique for determining temperatures and concentrations of hot combustion gases from infrared-emission spectra. Tech. rep., The Combustion Institute, Tenth Symposium on Combustion, 1965.

[8] FORD MOTOR COMPANY. *Engine ASY Chart 1999 V-Engines Manufacturing & Engineering Engine 4.6L-4V SN95.*

[9] HOCHHAUSER, A., BENSON, J., BURNS, V., GORSE, R., KOEHL, W., PAINTER, L., RIPPON, B., REUTER, R., AND RUTHERFORD, J. Effects of aromatics, mtbe, olefin and t90 on mass exhaust emissions from current and older vehicles - the auto/oil-air quality improvement program. Tech. Rep. SAE Paper 982444, Society of Automotive Engineers, 1998.

[10] ICHIKAWA, M., NONAKA, N., TAKADA, I., ISHIMORI, S., ANDOH, H., AND KUMAMOTO, K. Proton nmr analysis of octane number for motor gasoline: Part ii. *Applied Spectroscopy vol 45*, no 10 (1991).

[11] IPPOLITO, J. Statistical measurements and analysis of spark-ignition engine response to fuel additives via high-speed infrared imaging. Master's thesis, Rutgers University, 2005.

[12] JANSONS, M. *Simultaneous High-Speed Spectral and Infrared Imaging of Engine Combustion.* PhD thesis, Rutgers University, 2005.

[13] KOROLEV, V. N., MARUGIN, A. V., AND TSAREGRAKSII, V. B. Estimation of the petroleum product knock rating by regression analysis of near-infrared absorption spectra. *Technical Physics vol 45*, no 9 (2000), pp 90–95.

[14] LIN, S. *Artificial Intelligent Four Color Method, Stability Factor and Rutgers Animation Program.* PhD thesis, Rutgers University.

[15] MARONNA, R. A., MARTIN, R. D., AND YOHAI, V. J. *Robust Statistics Theory and Methods.* John Wiley and Sons, Inc, Hoboken, NJ, 2006.

[16] MOESER, P., AND HENTSCHEL, W. Development of a time resolved spectroscopic detection system and its application to automobile engines. Tech. Rep. SAE Paper 961199, Society of Automotive Engineers, 1996.

[17] PANDE, S. G., AND HARDY, D. R. A practical evaluation of published cetane indices. *Fuel vol 69*, issue 4 (1990), pp. 437–442.

[18] RHEE, K., AND CHANG, S. Empirical equations for adiabatic flame temperatures for some fuel-air combustion systems. *Combustion Science and Technology vol 44* (1985), pp 75–88.

[19] RODRIQUEZ-FORKER, A., UIHLEIN, J. P., SEGAL, J. S., SVERDRUP, G. M., SEYMOUR, J. P., KINATEDER, J. G., PIERCE, A., AND DURBIN, T. D. Fleet test using butane and propane mixtures. Tech. Rep. SAE Paper 982444, Society of Automotive Engineers, 1998.

[20] TARAZI, F. I. Development and fabrication of an optical access ford 4.6l v8 engine for internal combustion engine research. Master's thesis, Rutgers University, 1996.

[21] TAYLOR, A. B., MORAN, D. P., BELL, A. J., HODGSON, N. G., MYBURGH, I. S., AND BOTHA, J. J. Gasoline/alcohol blends: Exhaust emissions, performance and burn-rate in a multi-valve production engine. Tech. Rep. SAE Paper 961988, Society of Automotive Engineers, 1996.